Research Square

Preprints are preliminary reports that have not undergone peer review.
They should not be considered conclusive, used to inform clinical practice,
or referenced by the media as validated information.

Natural Radioactivity of Felsic Rocks of the Archaean Granite Greenstone Terrane of Bulawayo, Zimbabwe Craton

Robin Tinavo Mashingaidze

rtmashy@gmail.com

North-West University

Manny Mathuthu

North-West University

Innocent Mayida

North-West University

Research Article

Keywords: Natural radioactivity; Zimbabwe Craton, Archaean Granite Greenstone Terrane of Bulawayo, Gamma spectrometry

Posted Date: November 11th, 2026

DOI: https://doi.org/10.21203/rs.3.rs-11458328/v1

License: This work is licensed under a Creative Commons Attribution 4.0 International License.
Read Full License

Additional Declarations: No competing interests reported.

Natural Radioactivity of Felsic Rocks of the Archaean Granite Greenstone Terrane of Bulawayo, Zimbabwe Craton.

Robin Tinavo Mashingaidze [1, 2*], Manny Mathuthu [1] and Innocent Mayida [1, 3].

1. Centre for Applied Radiation Science and Technology (CARST), North-West University, Corner Albert Luthuli Road and University Drive, Mmabatho 2735, South Africa; manny.mathuthu@nwu.ac.za (M.M.); innomayida@gmail.com(I.M.)
2. Department of Earth Sciences, National University of Science and Technology (NUST), Corner Gwanda Road and Cecil Avenue, Ascot, Bulawayo P.O. Box AC939, Zimbabwe.
3. Radiation Protection Authority of Zimbabwe, 18 Armadale Road, Borrowdale West, Harare / P.O. Box A1710, Avondale, Harare, Zimbabwe

* Correspondence: rtmashy@gmail.com

Abstract

This study investigates the natural radioactivity and associated radiological hazards of felsic rocks in the Archaean Granite Greenstone Terrane of Bulawayo (AGGTB), Zimbabwe Craton. Firstly, the activity concentrations of the ^{238}U decay series, ^{232}Th decay series, and ^{40}K non series radionuclides in twenty four (24) representative felsic rock samples collected from the three main exposed felsic rock units in the AGGTB, namely younger porphyritic granites, fenitised granites and older gneissic granites were determined using a High Purity Germanium (HPGe) gamma-ray spectrometry detector system. Subsequently, the radiological hazard parameters quantifying the associated radiation exposure of its inhabitants to the ^{238}U decay series, ^{232}Th decay series and ^{40}K non series radionuclides within the exposed felsic rock units in the AGGTB were computed. The mean activity concentrations for the ^{238}U decay series, ^{232}Th decay series and ^{40}K non series radionuclides for the younger porphyritic granites were found to be 177.885 ± 0.009 Bq/kg, 252.261 ± 0.021 Bq/kg and 1422.178 ± 0.071 Bq/kg, respectively. The mean activity concentrations for the ^{238}U decay series, ^{232}Th decay series and ^{40}K non series radionuclides for the fenitised granites were found to be 137.788 ± 0.007 Bq/kg, 253.724 ± 0.021 Bq/kg and 1799.935 ± 0.087 B/kg, respectively. The mean activity concentrations for the ^{238}U decay series, ^{232}Th decay series and ^{40}K non series radionuclides for the older gneissic granites were found to be 40.889 ± 0.003 Bq/kg, 102.698 ± 0.009 Bq/kg and 1175.093 ± 0.063 Bq/kg, respectively. These results show that the natural radioactivity in the AGGTB, particularly in areas underlain by both the younger porphyritic granites and the fenitised granites may pose some radiological health risks to its inhabitants.

Key Words: Natural radioactivity; Zimbabwe Craton, Archaean Granite Greenstone Terrane of Bulawayo, Gamma spectrometry.

Introduction

On Earth human beings are continuously exposed to ionising radiation from both natural and anthropogenic sources. However, natural sources of radiation are widely recognised as the most significant means by which

human beings are exposed to ionising radiation sources (Zubair & Shafiqullah, 2020). The United Nations Scientific Committee on the Effects of Atomic Radiation (UNSCEAR) estimates that the world population's average annual effective dose from natural radiation sources is about 2.8 mSv (UNSCEAR, 2000). With the natural radiation exposures in human beings arising from both internal and external exposure pathways (Abdel Gawad et al., 2022). Internal exposures are due to inhalation of radionuclides which emit alpha, beta and gamma radiation inside the human body whereas external exposures are essentially due to the radioactive decay of radionuclides present in the environment (Salupeto-Dembo, 2020). Among the natural radiation sources contributing to external exposures, cosmic rays (i.e. cosmic radiation) and terrestrial radionuclides and their decay products (i.e. terrestrial radiation) are the largest contributors (Dina et al., 2022). The primary sources of cosmic radiation in the environment being the galaxies in outer space as well as the Sun. The interaction of these cosmic rays with atmospheric atoms results in the generation of secondary sources of extra-terrestrial radiation, i.e. cosmogenic radionuclides. Common cosmogenic radionuclides in our environment include: tritium (^{3}H), beryllium-7 (^{7}Be) and carbon-14 (^{14}C) (Laubenstein & Lawson, 2020). However, of these three commonly occurring cosmogenic radionuclides, only ^{3}H and ^{14}C contribute significantly to radiation exposure in human beings (Bajoga, 2016; Xhixha, 2013). However, only a minor component (about 0.4 mSv) of the world population's average annual effective dose from natural radiation sources at the Earth's surface is attributed to cosmic radiation sources (IAEA, 2004; UNSCEAR, 2000).

Thus the major contribution to natural background radiation at the Earth's surface is attributed terrestrial radiation, i.e. the radioactive of naturally occurring radionuclides present in the Earth. UNSCEAR estimates that the world population's average annual effective dose from terrestrial radiation is about 2.4 mSv (UNSCEAR, 2000). The terrestrial radiation contribution is mainly due to the radioactive decay of the uranium-238 (^{238}U) and thorium-232 (^{232}Th) decay series as well as the non-series potassium-40 (^{40}K) (Isinkaye & Emelue, 2015; Sharma, 2025). Since, ^{40}K is the only radioactive isotope of potassium, the gamma rays emitted from its radioactive decay can be used to estimate the concentrations of potassium present in the natural environment. However, the radioactive decay of the ^{238}U and ^{232}Th series towards stable end members, ^{206}Pb and ^{208}Pb, respectively are accompanied by the emission of alpha, beta and gamma radiation (Cinelli et al., 2019). Both the ^{238}U and ^{232}Th decay series are typically long and complex, for example, the ^{238}U decay series which is the longest natural decay chain, decays into stable ^{206}Pb via fourteen decays (eight alpha decays and six beta decays) (Eikenberg, 2002). However, both the ^{238}U and ^{232}Th naturally occurring radionuclides are not primary gamma emitters, being themselves alpha emitters. As a result the terrestrial gamma radiation contribution attributed to these two primordial radionuclides is based on gamma-rays emitted by their daughter products, not from the ^{238}U and ^{232}Th radionuclides themselves (alpha emitters). Therefore, the concentrations of the ^{238}U and ^{232}Th radionuclides in the environment can be measured using gamma-ray spectrometry related to their respective gamma-emitting progeny. Such measurements are accurate, provided the ^{238}U and ^{232}Th radionuclides are in secular equilibrium with their respective gamma-emitting daughter products (Alharbi, 2016; Cinelli et al., 2019; IAEA, 2003; Khan et al., 2023). Because these major contributors to terrestrial gamma radiation exposures in human beings, i.e. ^{238}U, ^{232}Th and ^{40}K radionuclides are characterised by relatively long half-lives that are comparable to the age of the Earth, they are often present in measurable concentrations in the environment (Plant et al., 1999). However, these dominant terrestrial gamma radionuclides are present in variable amounts in our environment, i.e. their concentrations vary from place to place, mainly according to

geology (Bezuidenhout, 2019; Kerur et al., 2010; UNSCEAR, 2000). Generally, for rocks, an increase in silica (SiO_2) content results in an increase in the concentrations of these dominant terrestrial radionuclides in the environment as well (Mason & Moore, 1982). Therefore, areas that are predominantly underlain by granitic or felsic rich rocks generally contain higher natural background radiation levels compared to areas predominantly underlain by mafic or sedimentary rocks (Akingboye & Ademila, 2019).

Since granitic rocks are the most abundant rocks of mountain belts and continental shield regions (Kerur et al., 2010), around the world there are several regions characterised by high concentrations of terrestrial radionuclides. Still, there are very few regions in the world which have anomalously high levels of natural background radiation; such regions are commonly referred to as high background radiation areas (HBRAs). Notable HBRAs in the world include: Yangjiang in China, Guarapari in Brazil, Karunagappally in India as well as Ramsar and Mahallat in Iran (Sreedharan & Geetha, 2016). The HBRAs in Brazil, China and India are all attributed to the presence of monazite, i.e. a reddish-brown phosphate mineral which is a significant source of rare earth elements, whilst the HBRAs at both Ramsar and Mahallat in Iran are attributed to the presence of anomalously high concentrations of radium-226 (^{226}Ra) and its daughter products, which are brought to the Earth's surface by hot sulphurous springs (Sohrabi, 2013; UNSCEAR, 2018). Therefore, inhabitants of some of these HBRAs can receive annual effective doses due to natural background radiation that are above the safety limit of 1 mSv recommended for the public by the International Centre for Radiological Protection (ICRP) (ICRP, 1991). Owing to the health risks associated with the exposure to natural background radiation, most countries across the world are now routinely monitoring the natural background radiation levels in their environment, especially radon (Aghdam et al., 2021).

However, in the Southern African nation of Zimbabwe very little is known concerning the occurrences and distributions of naturally occurring radionuclides across the country. This is despite the fact that the country is predominantly underlain by an exposed basement complex known as the Zimbabwe Craton, which is characterised by a high proportion of granites relative to greenstones of ~ 5:1 (Jelsma & Dirks, 2000). Thus the Zimbabwe Craton, like other Archaean cratons elsewhere in the world is characterised by a preponderance of outcropping granitic rock units of various ages and compositions which are typically enriched in uranium, thorium and potassium radioelements, suggesting that its inhabitants may be exposed to high natural background radiation. Thus radionuclides activity concentrations and distributions measurements across the Zimbabwe Craton are particularly important in terms of determining the natural background radiation exposure to the inhabitants. The present study investigates the natural radioactivity and associated radiological hazards of the main exposed felsic rocks in one of Zimbabwe's numerous Archaean Granitic Greenstone Terranes, in this case the Archaean Granite Greenstone Terrane of Bulawayo (AGGTB).

Regional Geological Setting of the Archaean Granite-Greenstone Terrane of Bulawayo

The Bulawayo Greenstone Belt (BGB) is situated in the south-central portion of the Zimbabwe Craton. Lithologically, typically of greenstone belts elsewhere in the world, the BGB consists of a supracrustal succession of volcanic and sedimentary rocks, i.e. volcano-sedimentary sequences, overlying the granitic-gneissic basement complex of the Zimbabwe Craton. In addition these volcano-sedimentary sequences in the BGB are marked by a low grade metamorphism, i.e. alteration of the basic volcanic rock mineral assemblages to green coloured chlorite-epidote-actinolite mineral assemblages (Hofmann et al., 2023). Structurally however,

the BGB forms a large tricuspate synclinorium of volcano-sedimentary successions which are both surrounded and locally intruded by older granitic-gneissic basement rocks and younger granitoid batholiths respectively (Hofmann et al., 2023). These intrusive younger granitoids batholiths, which are of varying compositions and ages, are believed to have been emplaced episodically within the BGB during a time span of at least 200 Ma, i.e. from ~ 2.7 Ga to 2.5 Ga. However, three distinct episodes of granitoid batholith emplacements can be recognised within the BGB (Garson, 1995). With the first recognised episode of granitoid emplacement in the BGB occurring at ~ 2.7 Ga, which resulted in the formation of massive granitic batholiths ranging in composition from plagioclase-rich trondhjemite and hornblende-bearing tonalite gneisses, and granodiorites, i.e. Tonalite-Trondhjemite-Granodiorite (TTG) batholiths. These sodium-rich TTG batholiths which are to be found widely scattered across the BGB are correlatives of the ~ 2.7 Ga Sesombi Suite of Granitoids of the Zimbabwe Craton (Wilson et al., 1995). In the BGB, these sodium-rich TTG batholiths are represented by the Esigodini (Essexvale) and Heany (Ncema) Tonalites (Garson, 1995). The second recognised episode of granitoid emplacement in the BGB is believed to have occurred at ~ 2.6 Ga, resulting in the formation of large potassium-rich porphyritic monzogranites batholiths. These potassium-rich porphyritic granitoids are correlatives of the ~ 2.6 Ga Chilimanzi Suite of Granitoids of the Zimbabwe Craton (Hofmann et al., 2023). In the BGB, these potassium-rich, i.e. potassic-rich granites porphyritic monzogranites are represented by the Matopo Adamellite and the Falls Road Porphyritic Granite (Garson, 1995). The last recognised episode of granitoid emplacement in the BGB is generally correlated with the period of widespread emplacement of discrete granitoid batholiths into an already consolidated, tectonically stable Zimbabwe Craton, which is believed to have occurred ~ 2.5 Ga. In the BGB, these relatively late-stage granitoid intrusions are represented by the Hillside Syenite Intrusion (HSI) (Garson, 1995). Thus, the BGB and its surrounding gneissic terrane and intruding Late Archaean granitoid batholiths together constitute the so called '*Archaean Granite-Greenstone Terrane of Bulawayo (AGGTB)* '.

Local Geological Setting of the Study Area

The study area comprises a significant portion of the Bulawayo City Council's Municipal Areas, i.e. the City of Bulawayo's built up areas or town-lands, and is situated between latitudes $20^0.02$' and $20^0.14$' South of the Equator and longitudes $28^0.30$' and $28^0.40$' East of the Greenwich Meridian. It covers an area that extends for approximately 140 km^2, with the Central Business District of Bulawayo (CBDB), situated approximately at its centre **(Figure 2.1**).

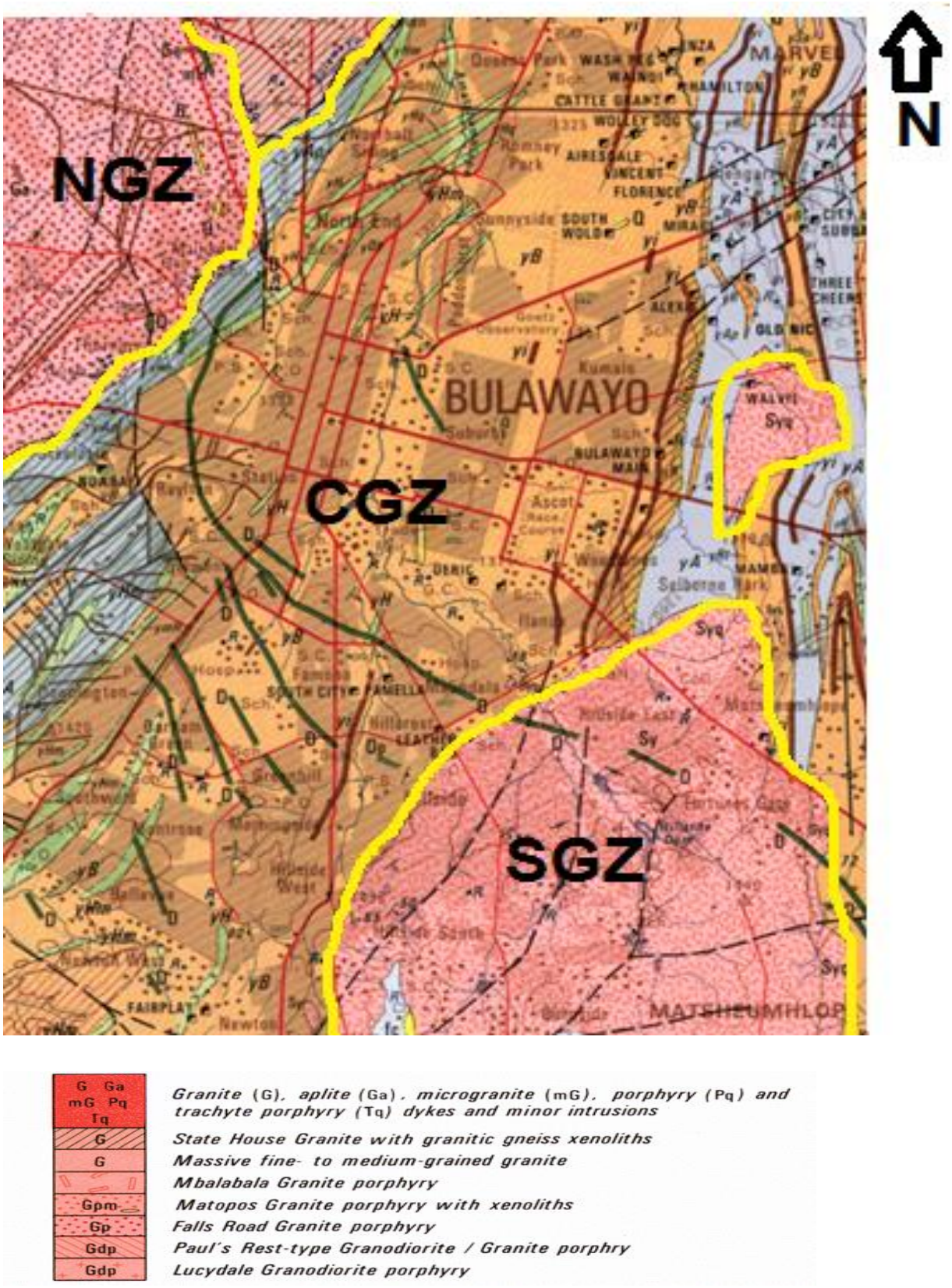


Figure 2. 1: Local Geological Map of the Study Area, showing a central greenstone zone separating two distinct granitic regions modified after (Garson, 1995; Turner, 1991).

Figure 2.1 shows that the study area can be broadly divided into three distinct geological regions, namely (i) the Northwestern Granitoid Zone (NGZ), (ii) the Southeastern Granitoid Zone (SGZ) and (iii) a Central Greenstone Zone (CGZ). With the areas predominantly underlain by granitic and syenitic rocks occupying the northwestern and southeastern regions of the study area, respectively and are separated from each other by a broad belt of greenstones (the predominant basalts and the volumetrically minor andesites) i.e. the Central Greenstone Zone (CGZ). In addition both the central greenstone belt and the granitic and syenitic rocks of the AGGTB are intruded by numerous Early Proterozoic mafic (dolerite) dykes and sills, belonging to the Umkondo Group (Garson, 1995).

Materials, Equipment and Methods

Rock Sample Collection and Preparation Procedures

Three principal felsic lithotypes are recognised in the study area, namely: (i) the younger porphyritic granites in the NGZ, (ii) the older gneissic granites in the NGZ and (iii) the syenites (fenitised granites) in the SGZ **(Figure 3.1 to Figure 3.3).**



Figure 3.1: Representative coarse grained younger porphyritic granite hand specimen from the NGZ.



Figure 3.2: Representative purplish-brown, fine to medium grained gneissic granite hand specimen from the NGZ. *NB: Faint foliation displayed by a preferred orientation of elongate quartz and trails of pale green acicular hornblende and pale brown, partly chloritized biotite (i.e. the gneissic granites are also spotted with green chlorite.)*



Figure 3.3: Representative porphyritic syenite hand specimen from the SGZ. *NB: Visualize the medium to coarse grained reddish (pinkish) feldspar-rich rock with, a porphyritic texture.*

A total of twenty four (24) representative felsic rock samples were collected from different representative granitic and syenitic outcrops throughout the AGGTB, namely: fifteen (15) younger porphyritic granites rock samples and four (4) older gneissic granites rock samples from the NGZ and five (5) porphyritic quartz syenites, i.e. fenitised granites rock samples from the SGZ. In addition an extra (1) tonalitic granitic sample was collected from the ruins of the collapsed old Riverside/Buena Vista Dam embankment, i.e. felsic rock sample which is foreign to both the granitic rock units of the NGZ and SGZ, to be used as the control sample **(Figure 3.1).** The

collected 25 felsic rock samples were thoroughly cleaned with distilled water to remove any potential sources of contamination brought from the field. The felsic rock samples were then later left to dry overnight in a laboratory oven at 110 ^{0} C to remove any moisture from the felsic rock samples (Omonya, 2021). These representative felsic rock samples were then later milled to yield fine grain powdered felsic rock samples using a laboratory ball mill.

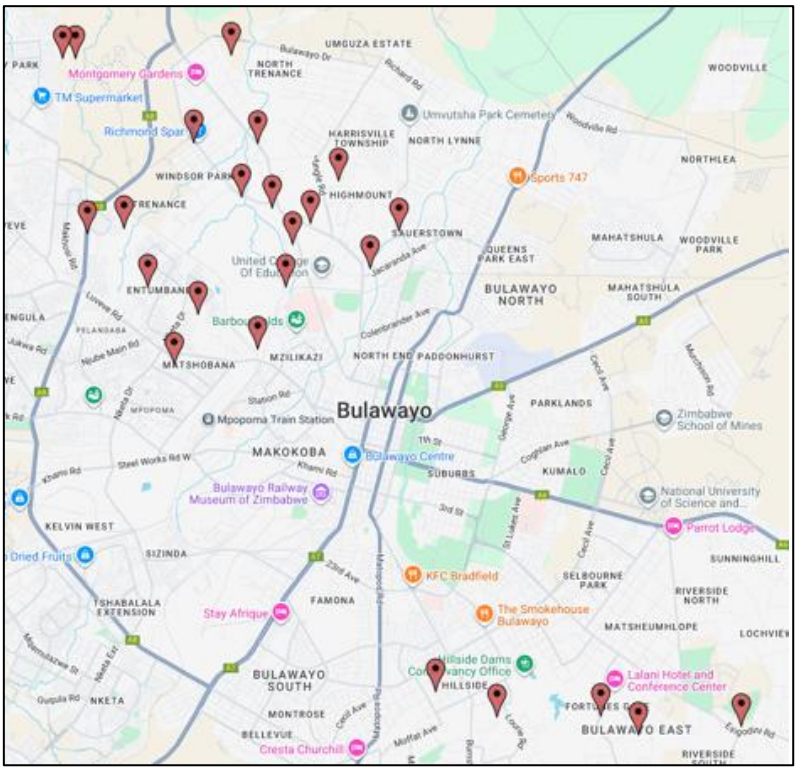


Figure 3.1: Study area terrain base map showing the representative felsic rock sample locations in the AGGTB.

Gamma Spectrometric Measurements

Prior to gamma-ray spectrometry analyses, the powdered felsic rock samples were kept for a period of at least 30 days in hermetically sealed Marinelli beakers to ensure that secular radioactive equilibrium conditions were established between ^{226}Ra, ^{222}Rn and its progeny before counting (Isinkaye & Emelue, 2015; Khan et al., 2023). After achieving secular radioactive equilibrium conditions, the gamma-ray spectrometry analyses were carried out at the Radiation Protection Authority of Zimbabwe (RPAZ) - Radiochemistry Laboratory, Harare using a cylindrical co-axial High Purity Germanium (HPGe) gamma-ray spectrometry detector system from Mirion Technologies (Canberra) Model GX4020. The electrically cooled GX4020 HPGe detector has an energy resolution, i.e. full width at half maximum (FWHM) of 2.0 keV at 1.33 MeV and 1.10 keV at 122 keV, respectively for cobalt-60, with relative efficiency of 40 %. The GX4020 HPGe detector has a 10 cm lead shielding on all sides with inner copper and tin lining to achieve the lowest possible background level. The HPGe detector's efficiency calibration was carried out using the Laboratory Sourceless Calibration Software (LabSOCS), run through Canberra's Genie 2000 Software, and cross-checked against measured efficiencies from certified point sources at four reference energies (122, 662, 1173, and 1332 keV). A simplified cylindrical Marinelli beaker geometry configuration with a sample filling height (FH) of 35 mm was selected for the

HPGe detector's efficiency calibration process. The gamma-ray spectra were acquired and analysed using the Canberra Genie 2000 Software (Canberra, 2006). The gamma-ray spectra of each sample were measured for a period of 172800 s. However prior to the samples measurements the environmental gamma background radiation at the laboratory was determined using a Marinelli beaker filled with non-radioactive deionised water under identical measurement conditions and later subtracted from the measured gamma ray spectra of each sample. The following gamma-ray photo peaks were utilised for the activity concentrations analyses of the ^{238}U decay series, ^{232}Th decay series and ^{40}K non series radionuclides:

(i) Uranium (^{238}U): Assuming secular equilibrium conditions between the ^{238}U-parent and progeny nuclides, i.e. ^{226} Ra and decay products ^{214}Pb and ^{214}Bi. The activity concentration of the ^{238}U was then determined indirectly from the specific gamma-ray emission lines of the ^{226}Ra progeny: ^{214}Pb at 295.21 keV (19.20 %) and 351.92 keV (37.20 %) and ^{214}Bi at 609.31 keV (46.30 %) and 1120.29 keV (15.10 %), respectively.

(ii) Thorium (^{232}Th): Assuming secular equilibrium conditions between the ^{232}Th-parent and progeny nuclides, i.e. ^{212}Pb and ^{228}Ac-progeny, the activity concentration of ^{232}Th was then determined indirectly from the specific gamma-ray emission lines of its progeny: ^{212}Pb at 238.63 keV (44.60 %) and ^{228}Ac at 338.32 keV (11.40 %), 911.60 keV (27.70 %) and 969.11 keV (16.60 %), respectively.

(iii) Potassium (^{40}K): This was measured directly from the analysis of its specific gamma-ray emission line at 1460.81 keV (10.67 %).

As a result the activity concentrations of the ^{238}U decay series radionuclides were calculated as the weighted arithmetic mean of the activity concentrations of the gamma-emitting ^{214}Pb and ^{214}Bi radionuclides calculated using the Genie 2000 Software. Accordingly, the ^{238}U decay series radionuclides activity concentrations uncertainties in the analysed granitic rock samples were calculated as:

$$\Delta^{238}\text{U decay series} = ((\Delta\ ^{214}\text{Bi})^2 + (\Delta^{214}\text{Pb})^2)^{1/2} \quad \textbf{(3.1)}$$

where Δ^{214}Bi and $\Delta\ ^{214}$Pb are the uncertainties associated with the activity concentrations of the ^{214}Bi and ^{214}Pb radionuclides, respectively calculated using the Genie 2000 Software.

Similarly, the activity concentrations of the ^{232}Th decay series radionuclides were derived based on the assumptions of secular radioactive equilibrium conditions in the ^{232}Th radionuclide and its progeny, in this case ^{212}Pb and ^{228}Ac radionuclides. Thus, in this study the activity concentrations of the ^{232}Th decay series radionuclides were calculated as the weighted arithmetic mean of the activity concentrations of the gamma-emitting ^{212}Pb and ^{228}Ac radionuclides calculated using the Genie 2000 Software. Accordingly, the ^{232}Th decay series radionuclides activity concentrations uncertainties in the analysed granitic rock samples were calculated as:

$$\Delta^{232}\text{Th decay series} = ((\Delta^{228}\text{Ac})^2 + (\Delta\ ^{212}\text{Pb})^2)^{1/2} \quad \textbf{(3.2)}$$

where Δ^{228}Ac and $\Delta\ ^{212}$Pb are the uncertainties associated with the activity concentrations of the ^{228}Ac and ^{212}Pb radionuclides, respectively calculated using the Genie 2000 Software.

Computation of Radiological Hazard Parameters

The following radiological parameters were determined for this study using the activity concentrations data obtained from the gamma spectrometry analyses of the representative granitic rock samples from the AGGTB: (i) the absorbed gamma dose rate in air (D), (ii) the annual effective dose equivalent (AEDE), (iii) the radium equivalent activity concentration index (Ra_{eq}), (iv) the external hazard index (H_{ext}), (v) the excess lifetime cancer risk (ELCR).

The absorbed gamma dose rate in air (D)

The absorbed gamma dose rate (nGy/h) in air from exposure to the three dominant naturally occurring radionuclides at 1 m above the ground in the AGGTB were determined from the activity concentrations of ^{226}Ra, ^{232}Th and ^{40}K, using (**Equation 3.3)**.

$$\boldsymbol{D\left(\frac{nGy}{h}\right) = 0.462A_{Ra-226} + 0.604A_{Th-232} \quad + 0.0417A_{K-40}} \qquad \boldsymbol{(3.3)}$$

where $A_{Ra\text{-}226}$, $A_{Th\text{-}232}$ and $A_{K\text{-}40}$ are the activity concentrations of ^{226}Ra (^{238}U) assuming secular equilibrium conditions in the ^{238}U decay series, ^{232}Th decay series and ^{40}K, respectively (expressed in Bq/kg) and 0.462, 0.604 and 0.0417 are their respective dose conversion factors. These radionuclide dose conversion factors are expressed in units of nGy/h per Bq/kg (UNSCEAR, 2000).

The annual effective dose equivalent (AEDE)

The annual effective dose equivalent (AEDE) provides a means to express the irradiated dose of the human body from the naturally occurring radionuclides. The outdoor annual effective dose equivalent rates were calculated using **(Equation 3.4)** (UNSCEAR, 2000).

$$\boldsymbol{AEDE\left(\frac{mSv}{y}\right) = Absorbed\ dose\left(\frac{10^{-9}Gy}{h}\right) x\ 8760(h) x 0.2\ x \frac{0.7x10^{-6}Sv}{Gy}} \qquad \boldsymbol{(3.4)}$$

where 0.7 Sv/Gy is the factor which is used to convert absorbed dose rate in nGy/h to equivalent effective dose rate in mSv/y, and 0.2 is occupancy factor, i.e. the proportion of the average time spent outdoors by an individual (UNSCEAR, 2000).

Radium Equivalent Activity Concentration Index (Ra_{eq})

Since the distribution of the three dominant naturally occurring radionuclides, i.e. ^{238}U decay series, ^{232}Th decay series and ^{40}K, is not uniform in the Earth's crust, the effects of these radionuclides on human beings also vary from one radionuclide to another. Therefore in order to assess the combined radiological risk posed by these naturally occurring radionuclides, the radium equivalent activity index (Ra_{eq}) was determined using Equation 3.5:

$$\boldsymbol{Ra_{eq}\left(\frac{Bq}{kg}\right) = A_{U-238} + 1.43\ A_{Th-232} + 0.077A_{K-40}} \qquad \boldsymbol{(3.5)}$$

where $A_{U\text{-}238}$, $A_{Th\text{-}232}$ and $A_{K\text{-}40}$ are the activity concentrations of the ^{238}U, ^{232}Th and ^{40}K radionuclides, respectively (expressed in Bq/kg). The maximum allowed value of Ra_{eq} is 370 Bq/kg, which is the equivalence of an annual gamma radiation dose of 1.5 mSv/y (Baz et al., 2015).

External hazard index (H_{ex})

In order to ensure that the external radiation exposure due to the ^{238}U decay series, ^{238Th} decay series and ^{40}K non series radionuclides in the analysed granitic rock samples from the AGGTB is within the recommended annual dose equivalent of 1 mSv/y, the external hazard index, H_{ex} was determined using **(Equation 3.6):**

$$H_{ex} = \frac{A_{U-238}}{370} + \frac{A_{Th-232}}{259} + \frac{A_{K-40}}{4810} \leq 1 \qquad (3.6)$$

where $A_{U\text{-}238}$, $ATh_{\text{-}232}$ and $A_{K\text{-}40}$ are the mean activity concentrations of the ^{238}U decay series, ^{232}Th decay series and ^{40}K non series radionuclides, respectively. The radiation hazard is generally considered insignificant when the value of H_{ex} is lower than unity, i.e. the equivalence of the maximum allowable radium equivalent activity of 370 Bq/kg (OECD, 1979).

The Excess Lifetime Cancer Risk (ELCR)

The probability of inhabitants of the AGGTB developing cancer as a result of lifetime exposure to ionizing radiation from the naturally occurring radionuclides in their environment, i.e. the excess lifetime cancer risk (ELCR) was determined using **(Equation 3.7)** (UNSCEAR, 2000):

$$ELCR = AEDE \times DL \times RF \qquad (3.7)$$

where *AEDE* is the annual effective dose equivalent, *DL*, is the average lifespan of human beings, typically 70 years and *RF* is the risk factor of fatal cancer per Sievert which is 0.05 Sv^{-1} for stochastic effects based on the recommendations of the ICRP60 for the general public (ICRP, 1991).

Results and Discussion

Gamma-ray spectrometric characteristics of the felsic rock units in the Archaean Granite-Greenstone Terrane of Bulawayo

The gamma-ray spectrometric characteristics of the three dominant felsic rock units in the AGGTB are presented separately in the following sections.

Activity concentrations of naturally occurring radionuclides in the Northwestern Granitic Zone

The activity concentrations of the naturally occurring radioactive radionuclides, namely the ^{238}U decay series, ^{232}Th decay series and ^{40}K non series radionuclides, in four selected representative older gneissic granitic rock samples from the AGGTB, which were measured using the GX4020 HPGe detector, are presented in **Table 4.1.** The activity concentrations of the ^{238}U decay series radionuclides in the gneissic granites, varied from 34.428 ± 0.003 Bq/kg, obtained for the flat gneissic granitic rock pavements at High Mount to 51.631 ± 0.003 Bq/kg, obtained for the exposed gneissic granitic rock outcrops, a few metres from the confluence of the

Matsheumhlope stream and the Bulawayo Spruit at Sauerstown, with an average value of 40.889 ± 0.003 Bq/kg for the entire region. The activity concentrations of the ^{232}Th decay series radionuclides for the gneissic granites rock varied from 74.725 ± 0.007 Bq/kg, obtained at High Mount to 113.970 ± 0.010 Bq/kg, obtained for the weathered gneissic granitic pavements next to the Breedon Everad, with an average value of 102.698 ± 0.009 Bq/kg for the entire region. Lastly, the ^{40}K non series radionuclides activity concentrations in the gneissic granites varied from 1126.872 ± 0.062 Bq/kg obtained at Highmount to 1225.579 ± 0.066 Bq/kg recorded at Sauerstown, with a mean value of 1175.093 ± 0.063 Bq/kg for the entire region.

Table 4. 1: Activity concentrations of the ^{238}U series, ^{232}Th series and ^{40}K non series radionuclides in areas underlain by the older gneissic granites in the NGZ.

Sample Name	Sample Locality	Mean activity ^{238}U decay series (Bq/kg)	Mean activity ^{232}Th decay series (Bq/kg)	Mean activity ^{40}K non series (Bq/kg)
AGGTB1	High Mount	34.428 ± 0.003	74.725 ± 0.007	1126.872 ± 0.062
AGGTB2	Sauerstown	39.909 ± 0.003	111.301 ± 0.009	1225.579 ± 0.066
AGGTB3	Breedon Everard	37.587 ± 0.003	113.970 ± 0.010	1219.295 ± 0.065
AGGTB4	Sauerstown	51.631 ± 0.003	110.794 ± 0.009	1128.624 ± 0.059
Average± Standard Error		**40.889 ± 0.003**	**102.698 ± 0.009**	**1175.093 ± 0.063**

The activity concentrations of the ^{238}U decay series, ^{232}Th decay series and ^{40}K non series radionuclides obtained from the GX4020 HPGe detector analyses of fifteen (15) selected representative younger porphyritic granitic rock samples from the NGZ are given in **Table 4.2.** The activity concentrations of the ^{238}U decay series radionuclides in the younger porphyritic granites, varied from 77.778 ± 0.005 Bq/kg obtained at Princess Margaret Outcrops, Richmond to 304.644 ± 0.015 Bq/kg obtained at Richmond, with an average value of 177.885 ± 0.009 Bq/kg. The ^{232}Th decay series radionuclides activity concentrations in the younger porphyritic granites varied from 207.545 ± 0.017 Bq/kg obtained at Cowdray Park to 313.198 ± 0.025 Bq/kg obtained at the younger porphyritic granite outcrops exposed along the Old Victoria Falls Road, with an average value of 252.261 ± 0.021 Bq/kg for the entire region. Lastly the ^{40}K non series radionuclides activity concentrations in the younger porphyritic granites varied from 1065.958 ± 0.057 Bq/kg obtained at Emakhandeni to 1819.024 ± 0.092 Bq/kg obtained at Mzilikazi, with a mean value of 1422.178 ± 0.071 Bq/kg for the entire region.

Table 4.2: Activity concentrations of ^{238}U decay series, ^{232}Th decay series and ^{40}K non series radionuclides in areas underlain by the younger porphyritic granites in the NGZ.

Sample	**Locality**	**Mean activity ^{238}U decay series (Bq/kg)**	**Mean activity ^{232}Th decay series (Bq/kg)**	**Mean activity ^{40}K non series (Bq/kg)**
AGGTB5	Old Falls Road	243.790 ± 0.011	313.198 ± 0.025	1393.338 ± 0.058
AGGTB6	Mzilikazi	241.822 ± 0.012	248.330 ± 0.021	1819.024 ± 0.092
AGGTB7	Richmond	304.644 ± 0.015	304.359 ± 0.025	1792.206 ± 0.092
AGGTB8	Mpopoma	171.195 ± 0.009	274.937 ± 0.023	1181.416 ± 0.061
AGGTB9	Entumbane	118.855 ± 0.007	247.339 ± 0.020	1451.328 ± 0.076
AGGTB10	Richmond	204.272 ± 0.011	281.272 ± 0.023	1556.740 ± 0.080
AGGTB15	Barbourfields	253.932 ± 0.013	249.533 ± 0.021	1447.154 ± 0.079
AGGTB16	Cowdray Park	123.220 ± 0.007	207.545 ± 0.017	1426.892 ± 0.073
AGGTB17	Cowdray Park	93.649 ± 0.006	210.108 ± 0.017	1512.771 ± 0.078
AGGTB18	Emakhandeni	158.405 ± 0.007	225.212 ± 0.018	1505.532 ± 0.063
AGGTB19	Emakhandeni	285.825 ± 0.014	216.551 ± 0.018	1065.958 ± 0.057
AGGTB21	Manyewu	98.316 ± 0.006	234.953 ± 0.020	1644.635 ± 0.085
AGGTB22	Richmond	136.478 ± 0.006	229.363 ± 0.018	1139.660 ± 0.048
AGGTB23	Glenville	156.092 ± 0.008	291.948 ± 0.024	1210.417 ± 0.064
AGGTB24	Richmond	77.778 ± 0.005	249.272 ± 0.021	1185.604 ± 0.063
Average ± Standard Error		**177.885±0.009**	**252.261 ± 0.021**	**1422.178 ± 0.071**
Range		**77.778 ± 0.005** **304.644 ± 0.015**	**207.545 ± 0.017** **313.198 ± 0.025**	**1065.958 ± 0.057** **1819.024 ± 0.092**

The activity concentrations of the ^{238}U decay series, ^{232}Th decay series and ^{40}K non series radionuclides obtained from the GX4020 HPGe gamma-ray spectrometry analyses of five (5) selected representative fenitised granitic rock samples, i.e. porphyritic quartz syenite rock samples are presented in **Table 4.3**. The activity

concentrations of the ^{238}U decay series radionuclides in the fenitised granites, varied from 63.305 ± 0.004 Bq/kg at Hillside to 215.825 ± 0.011 Bq/kg at Mqabukho Heights, with an average value of 137.788 ± 0.007 Bq/kg. The ^{232}Th decay series radionuclides activity concentrations in the fenitised granites, varied from 132.746 ± 0.011 Bq/kg at Hillside to 427.746 ± 0.035 Bq/kg at Hillside, with a mean value of 253.724 ± 0.021 Bq/kg. Lastly the ^{40}K non series activity concentrations varied from 1555.469 ± 0.079 Bq/kg at Fortunes Gate to 1980.095 ± 0.083 Bq/kg at an abandoned quarry mine at Burnside, with a mean value of 1799.935 ± 0.087 Bq/kg. With these distinctive high ^{40}K non series activity concentrations, reflecting basically the feldspathic nature of the fenitised granites in the SGZ, i.e. the presence of major potassium silicate minerals in the syenites found in the SGZ, which consists of microcline-microperthite (75-90%) with subordinate finer grained microcline and albite-oligoclase (GSZ, 2024).

Table 4. 3: Activity concentrations of the ^{238}U decay series, ^{232}Th decay series and ^{40}K non series radionuclides in areas underlain by the fenitised granites, i.e. porphyritic quartz syenites in the SGZ**.**

Sample ID	**Locality**	**Mean activity ^{238}U decay series (Bq/kg)**	**Mean activity ^{232}Th decay series q/kg)**	**Mean activity ^{40}K (Bq/kg)**
AGGTB11	Hillside	206.475 ± 0.011	427.746 ± 0.035	1822.034 ± 0.090
AGGTB12	Hillside	63.305 ± 0.004	132.746 ± 0.011	1778.095 ± 0.088
AGGTB13	Burnside	106.538 ± 0.005	195.924 ± 0.016	1980.095 ± 0.083
AGGTB14	Fortunes Gate	96.798 ± 0.006	241.205 ± 0.020	1555.469 ± 0.079
AGGTB20	Mqabukho Heights	215.825 ± 0.011	271.001 ± 0.022	1863.981 ± 0.094
Average ± Standard Error		**137.788 ± 0.007**	**253.724 ± 0.021**	**1799.935 ± 0.087**
Range		**63.305 ± 0.004 - 215.825 ± 0.011**	**132.746 ± 0.011 - 427.746 ± 0.035**	**1555.469 ± 0.079 - 1980.095 ± 0.083**

Summary of activity concentrations of naturally occurring radionuclides in the felsic rock units of the Archaean Granite-Greenstone Terrane of Bulawayo

The study results show that both the younger porphyritic granites and the fenitised granites in the AGGTB contain enhanced concentrations of naturally occurring radionuclides. However, the fenitised granites generally have slightly higher concentrations of potassium (1799.935 ± 0.087 Bq/kg) compared to the younger porphyritic

granites (1422.178 ± 0.071 Bq/kg). This can be attributed to the presence of more potassium feldspars in the primary rock forming minerals of syenites compared to the porphyritic granites. For example, the porphyritic quartz syenites at Hillside have the potassium-rich alkali feldspar, microcline ($KAlSi_3O_8$) as the dominant feldspar in their groundmass (Garson, 1995). The activity concentrations of the three dominant radionuclides in all the three main exposed felsic rock units of the AGGTB are significantly higher than the worldwide average activity concentrations of 33 Bq/kg, 45 Bq/kg and 420 Bq/kg for the ^{238}U decay series, ^{232}Th decay series and ^{40}K non series radionuclides , respectively (UNSCEAR, 2000). The results presented in **Table 4.2 and Table 4.3** show that both the younger porphyritic granites and the fenitised granites have mean activity concentrations of both ^{238}U decay series and the ^{232} Th decay series radionuclides that are considerably higher than the world average values for granites of 42 Bq/kg and 73 Bq/kg, for ^{238}U and ^{232}Th decay series, respectively (Chen & Lin, 1996). This can be attributed to the presence of accessory minerals such as zircon, monazite, thorite and sphene in both the younger porphyritic and fenitised granites of the AGGTB. Such accessory minerals (i.e. zircon, monazite, thorite and sphene) are favourable hosts for both uranium and thorium in igneous rocks (Plant et al., 1999). In addition, the activity concentrations for the ^{40}K non series radionuclides obtained for both the younger porphyritic granites and the fenitised granites in this study of ~ 1422 Bq/kg and 1800 Bq/kg, respectively are considerably higher than the world average value for granites of 1055 Bq/kg (Chen & Lin, 1996). This can be attributed to the fact that potassium is a major element in the major rock forming minerals, e.g. potassium feldspars and micas that are dominant in Late Archaean granitoids from all over the world, which is also the case with both the younger porphyritic granites and the fenitised granites (syenites) in the AGGTB. For example, petrographically, the biotite bearing granites of the Matopos Granite Intrusion which are representative of the younger porphyritic granites in the AGGTB are principally comprised of microcline ($KAlSi_3O_8$) at ~ (34%), oligoclase $(Na,Ca)(Si,Al)_4O_8$ at ~ 33%, quartz (SiO_2) at ~ 27% and biotite $K(Mg,Fe)_3\ AlSi_3O_{10}(F,OH)_2$ at ~ 14% (Dumisa et al., 2024). Thus, potassium is a major element in both microcline and biotite, which are among the dominant rock forming minerals in the younger porphyritic granites in the AGGTB. In fact, the younger porphyritic granites in the AGGTB have microcline as the dominant feldspar in their groundmass, i.e. they are essentially potassic-rich porphyritic granites (Garson, 1995). Hence the regions underlain by the Late Archaean granitoid rocks in the AGGTB can largely be considered to be high natural background radiation regions. This is also in accordance with the published results from isotopic studies of selected granitoid rocks in Zimbabwe, which found evidence that the Zimbabwe Craton has a relatively higher-level radiogenic signature compared with other Archaean continental crustal regions (Taylor et al., 1984). Furthermore, the study results show that the activity concentration values of the ^{232}Th decay series radionuclides are consistently higher than those of the ^{238}U decay series radionuclides, over the entire study region i.e. across all the three dominant felsic lithotypes in the AGGTB. This is consistent with the distribution of these radioelements in the Earth's crust, where in general the relative abundance of uranium is considerably lower than that of thorium (Rikhvanov, 2019). The highest average activity concentration value of ^{40}K non series radionuclide of 1800 Bq/kg were obtained for the regions predominantly underlain by the fenitised granites in the SGZ, which is expected as the syenites are generally richer in potassium minerals, particularly potassium feldspars than the more mafic, plagioclase-rich younger porphyritic and gneissic granites in the NGZ. Conversely, the highest average activity concentration value of the ^{238}U decay series of 179 Bq/kg were obtained for the regions predominantly underlain by the younger porphyritic granites in the NGZ, which can be attributed to the fact that the younger porphyritic

granites contain more mafic minerals, such as biotite and amphiboles than both the fenitised and gneissic granites. In general these mafic minerals are known to contain some of the highest uranium contents in granites, for example the average uranium contents in both biotite and amphibole are known to be approximately, 36 ppm and 21 ppm, respectively (IAEA, 1989).

Variations of thorium and uranium elemental concentrations in the felsic rock units of the Archaean Granite-Greenstone Terrane of Bulawayo

The measured activity concentrations of the ^{238}U decay series in Bq/kg and the ^{232}Th decay series in Bq/kg in the analysed felsic rock samples in the AGGTB were converted to their respective (equivalent) elemental concentrations in parts per million, i.e. ppm. The elemental concentrations of uranium and thorium were ascertained using the IAEA recommended conversion factors, namely; 1 ppm U = 12.35 Bq/kg of ^{238}U, and 1 ppm Th = 4.06 Bq/kg of ^{232}Th (Christodoulides et al., 2003; IAEA, 2003). These estimates of the uranium and thorium elemental concentrations, derived on the assumption of equilibrium concentrations are henceforth reported as equivalent uranium (eU) and equivalent thorium (eTh) concentrations, respectively. The equivalent uranium and thorium elemental concentrations for the three dominant felsic lithotypes in the AGGTB are presented in **Table 4.4** to **Table 4.6. Table 4.4** shows that for the gneissic granites in the NGZ, the equivalent uranium concentrations varied from 2.79 to 4.18 ppm, with a mean value of 3.31 ± 0.53 ppm, whilst the equivalent thorium concentrations for these gneissic granites varied from 18.41 to 28.07 ppm, with a mean value of 25.30 ± 3.99 ppm. The variations of the equivalent uranium concentrations observed in the gneissic granites in the NGZ, i.e. ranging between 2.79 to 4.18 ppm are comparable with the reported global ranges of uranium abundance in granites and rhyolites, which range between 2 to 50 ppm (Tye et al., 2017). However, the average uranium abundance of 3.31 ± 0.53 ppm obtained for the gneissic granites in this study is slightly higher than the average uranium abundances in the Earth's crust of between 1 to 3 ppm (Cumberland et al., 2016). The variations of equivalent thorium concentrations observed in the gneissic granites in the NGZ, i.e. ranging between 18.41 to 28.07 ppm are within range of the reported global ranges of thorium abundance in granites and rhyolites, which ranges between 8 to 56 ppm (Tye et al., 2017). The average equivalent thorium abundance in the gneissic granites of 25.30 ± 3.99 ppm obtained in this study is slightly higher than the reported global average thorium abundance in the granites and rhyolites, which is typically around 10 ppm (Tye et al., 2017). **Table 4.4** also shows that the resultant eU/eTh ratios for the gneissic granites in the NGZ varied from 0.11 to 0.15, with a mean value of 0.13 ± 0.02**,** which is much lower than the average upper continental crust (UCC) eU/eTh ratio of 0.26 (Xhixha, 2013).

Table 4.4: Equivalent elemental concentrations of uranium, thorium (ppm) and elemental ratio of eTh/eU in areas underlain by the gneissic granites in the NGZ.

Sample ID	**Sample Locality**	**eU (ppm)**	**eTh (ppm)**	**eU/eTh**
AGGTB1	High Mount	2.79	18.41	0.15

AGGTB2	Sauerstown	3.23	27.41	0.12
AGGTB3	Breedon Everard	3.04	28.07	0.11
AGGTB4	Sauerstown	4.18	27.29	0.15
Average ± Standard Deviation		**3.31 ± 0.53**	**25.30 ± 3.99**	**0.13 ± 0.02**
Range		**2.79 to 4.18**	**18.41 to 28.07**	**0.11 to 0.15**

Table 4.5: Equivalent elemental concentrations of uranium, thorium (ppm) and elemental ratio of eTh/eU in areas underlain by the younger porphyritic granites in the NGZ.

Sample ID	**Locality**	**eU (ppm)**	**eTh (ppm)**	**eU/eTh**
AGGTB5	Old Falls Road	19.74	77.14	0.26
AGGTB6	Mzilikazi	19.58	61.17	0.32
AGGTB7	Richmond	24.67	74.97	0.33
AGGTB8	Mpopoma	13.86	67.72	0.21
AGGTB9	Entumbane	9.62	60.92	0.16
AGGTB10	Richmond	16.54	69.23	0.24
AGGTB15	Barbourfields	20.56	61.46	0.34
AGGTB16	Cowdray Park	9.98	51.12	0.20
AGGTB17	Cowdray Park	7.58	51.75	0.15
AGGTB18	Emakhandeni	12.83	55.47	0.23
AGGTB19	Emakhandeni	23.14	53.34	0.43
AGGTB21	Manyewu	7.96	57.87	0.14
AGGTB22	Richmond	11.05	56.49	0.20
AGGTB23	Glenville	12.64	71.91	0.18
AGGTB24	Richmond	6.30	61.40	0.10

Average ± Standard Deviation	**14.40 ± 5.74**	**62.13 ± 8.05**	**0.23 ± 0.09**
Range	**6.30 to 24.67**	**51.12 to 77.14**	**0.10 to 0.43**

Table 4.5 shows that for the younger porphyritic granites in the NGZ, the equivalent uranium concentrations varied from 6.30 to 24.67 ppm, with an average value of 14.40 ± 5.74 ppm, whilst the equivalent thorium concentrations for the younger porphyritic granites varied from 51.12 to 77.14 ppm, with a mean value of 62.13 ± 8.05 ppm. These variations of equivalent uranium concentrations observed in the younger porphyritic granites in the NGZ, i.e. ranging between 6.30 to 24.67 ppm are comparable with the reported global ranges of uranium abundance in granites and rhyolites, which range between 2 to 50 ppm (Tye et al., 2017). However, the average uranium abundance in the younger porphyritic granites of 14.40 ± 5.74 ppm obtained in this study is considerably higher than the average uranium abundance in the Earth's crust, which ranges between 1 to 3 ppm (Cumberland et al., 2016). The variations of equivalent thorium concentrations observed in the younger porphyritic granites in the NGZ, i.e. ranging between 51.12 to 77.14 ppm are slightly higher than the reported global ranges of uranium abundance in granites and rhyolites, which range between 8 to 56 ppm (Tye et al., 2017). However, the average abundance of thorium in the younger porphyritic granites of 62.13 ± 8.05 ppm is significantly higher than the reported global average thorium abundance in the granites and granodiorites of around 10 ppm (Tye et al., 2017). The resultant eU/eTh ratios for the younger porphyritic granites in the NGZ varied from 0.10 to 0.43, with a mean value of 0.23 ± 0.09, which is much closer to the average upper continental crust (UCC) eU/eTh ratio of 0.26 (Xhixha, 2013). This suggests that compositionally, i.e. geochemically the younger porphyritic granites are very similar to the average Earth materials found in the upper continental crust.

Table 4.6: Equivalent elemental concentrations of uranium, thorium (ppm) and elemental ratios of eTh/eU in areas underlain by the fenitised granites (porphyritic quartz syenites) in the SGZ.

Sample ID	**Locality**	**eU (ppm)**	**eTh (ppm)**	**eU/eTh (ppm)**
AGGTB11	Hillside	16.72	105.36	0.16
AGGTB12	Hillside	5.13	32.70	0.16
AGGTB13	Burnside	8.63	48.30	0.18
AGGTB14	Fortunes Gate	7.84	59.41	0.13
AGGTB20	Mqabukho Heights	17. 48	66.75	0.26
Average ± Standard Error		**11.16 ± 4.99**	**62.50 ± 24.31**	**0.18 ± 0.04**

Range	**5.13 to 17.48**	**32.70 to 105.36**	**0.13 to 0.26**

Table 4.6 shows that for the fenitised granites, i.e. porphyritic quartz syenites in the SGZ, the equivalent uranium concentrations varied from 5.13 to 17.48 ppm, with an average value of 11.16 ± 4.99 ppm, whilst the equivalent thorium concentrations for these porphyritic quartz syenites varied from 32.70 to 105.36 ppm, with a mean value of 62.50 ± 24.31ppm. The variations of equivalent uranium concentrations observed in the porphyritic quartz syenites in the SGZ, i.e. ranging between 5.13 to 17.48 ppm are comparable with the reported global ranges of uranium abundance in syenites and phonolites, which ranges between 0.1 to 26 ppm (Tye et al., 2017). However the average uranium abundance of 11.16 ± 4.99 ppm obtained for the porphyritic quartz syenites in this study is significantly higher than the average uranium abundance in the Earth's crust of between 1 to 3 ppm (Cumberland et al., 2016). The variations of equivalent thorium concentrations observed in the porphyritic quartz syenites in this study, i.e. ranging between 32.70 and 105.36 ppm, are significantly higher than the reported global ranges of thorium abundance in syenites and phonolites, which are between 0.7 and 35 ppm (Tye et al., 2017). Thus, the average thorium abundance in the porphyritic quartz syenites of 62.13 ± 8.05 ppm obtained in this study is significantly higher than the reported global average thorium abundance in the syenites and phonolites, which is typically around 10 ppm (Tye et al., 2017). The resultant eU/eTh ratios for the porphyritic quartz syenites in the SGZ varied from 0.13 to 0.26, with a mean value of 0.18 ± 0.04, which is lower than the average upper continental crust (UCC) eU/eTh ratio of 0.26 (Xhixha, 2013).

Summary of thorium and uranium elemental concentrations in the felsic rock units of the Archaean Granite-Greenstone Terrane of Bulawayo

The results from the study have shown that the lowest average equivalent uranium and thorium concentrations in the AGGTB were encountered in the areas underlain by gneissic granites, with observed average equivalent uranium and thorium concentrations of 3.31 ppm and 25.30 ppm, respectively, whilst the highest average equivalent uranium and thorium concentrations in the AGGTB were observed in the areas that are underlain by both the younger porphyritic granites and the porphyritic quartz syenites. However, the equivalent average uranium and thorium concentrations obtained in the younger porphyritic granites and porphyritic quartz syenites are comparable, for example the average equivalent thorium concentration for the porphyritic quartz syenites is 62.50 ppm whilst for the younger porphyritic granites its 62.13 ppm. These findings are consistent with the suggestion of other researchers that both the porphyritic quartz syenites in the SGZ and the younger porphyritic granites in NGZ were derived from the same parent magma, i.e. both formed from the magmatic differentiation and fractionation processes associated with the Matopos Porphyritic Granite Intrusion Event (MPGIE) (Amm, 1965) Thus, both the porphyritic quartz syenites and the younger porphyritic granites in the AGGTB share remarkable geochemical properties, as confirmed by their comparable uranium and thorium concentrations obtained in this study. Globally, thorium is expected to be at least four times as abundant as uranium in most igneous rocks (Mareschal, 2014). This is consistent with the findings from this study, where the eTh/eU for both the porphyritic quartz syenites and younger porphyritic granites are, 5.60 and 4.31, respectively**.** In the AGGTB, the average equivalent thorium concentrations are highly variable (25.30 ppm – 62.13 ppm), with the lowest average value of 25.30 ppm associated with the gneissic granites in the NGZ and the highest average value of

62.50 ppm associated with the porphyritic quartz syenites in the SGZ. However, the eU/eTh ratios in all the three dominant felsic lithotypes in the AGGTB were found to be lower than the average upper continental crust (UCC) value of 0.26 (Xhixha, 2013). These low eU/eTh values obtained for the felsic samples further providing evidence for uranium mobilization/migration in the AGGTB, possibly as a result of the oxidative weathering and alteration of its ancient parent granitic rocks. Generally, in an oxidizing environment, compounds of thorium remain almost insoluble in aqueous solution, while uranium compounds are much better soluble (Eikenberg, 2002). For example, the lowest average eU/eTh value of 0.13 is associated with the older gneissic granites in the NGZ. These low average values of eU/eTh for the older gneissic granites suggest that they are affected by hydrothermal alteration as evidenced by the presence of sericite and chlorite in their primary rock-forming minerals. The average uranium concentrations of 11.16 ppm and 14.40 ppm obtained for the porphyritic quartz syenites, and younger porphyritic granites are much higher than the expected average uranium concentration for granites of 4 ppm (Nishimori et al., 1977). At the same time, the average thorium concentrations of 62.13 and 62.50 ppm obtained for the younger porphyritic granites and the porphyritic quartz syenites, respectively in the AGGTB, are much higher than the expected average thorium concentration for granites of 12 ppm (Nishimori et al., 1977). Finally, the fact that the average eU/eTh ratios for all the felsic lithotypes in the study area are less than 0.29 (i.e. which corresponds to an eTh/eU ratio of 3.5), suggests considerable thorium enrichment and/ or potential uranium leaching in the AGGTB, which is characteristic of Archaean erosional landsurfaces, particularly in regions of deep tropical weathering conditions like Zimbabwe.

Comparison of the average radioelement concentrations of the felsic rocks units in the Archaean Granite-Greenstone Terrane of Bulawayo with those in other cratons.

Since Archaean Granite-Greenstone Terranes occur in many Archaean cratonic regions of the world, we compared the average activity concentrations of the radionuclides obtained in this study with published data from other ancient cratonic regions of the world. However, since there are about 35 cratonic segments of varying ages and compositions exposed at the present-day continental surface (Carlson et al., 2019), we only consider the distributions of radioelements in some of the cratonic segments associated with the ancient supercontinent Gondwana. The ancient supercontinent Gondwana was comprised of present-day continental landmasses of South America, Africa, Madagascar, Peninsular India, New Zealand, Australia and Antarctica (Craddock, 1990). The African Shield, i.e. present-day Africa comprises five former Gondwana cratonic segments, namely the Kalahari Craton, the West African Craton, the Congo Craton, the East Saharan Craton and the Arabian-Nubian Craton (Goodwin, 1996). For Peninsular India, the five largest former Gondwana cratonic segments include the Singhbhum Craton, the Aravalli Craton, the Bundelkhand Craton, Bastar Craton and the Dharwar Craton (Manikyamba et al., 2024; Rajesh et al., 2009). Similarly, South America can be divided into four large cratonic segments. The largest cratonic segments in South America are the Sao Francisco and the Amazonian Cratons. However, there are numerous other smaller cratonic segments such as the Luiz Alves, Rio de La Plata and Sao Luiz Cratons (Barretto & Tassinari, 1992). These former ancient Gondwana cratonic segments are all representative of typical Archaean Granite Greenstone Terranes. However, the Kaapvaal Craton of South Africa (3.6 – 3.0 Ga) is one of the ancient Gondwana cratonic segments generally considered to be closely related with the Zimbabwe Craton both spatially and temporal. These two ancient Gondwana cratonic segments are comprised of diverse types of Archaean granitoids whose tectonic rock units share remarkable

geochemical similarities. Moyen et al. (2021) investigated the spatial distribution of potassium, uranium and thorium in the Heerenveen Batholith of the Barberton Granite-Greenstone Terrane, Kaapvaal Craton of South Africa by means of gamma-ray spectrometry **(Table 4.7).**

Table 4. 7: Average concentrations of radioelements in selected former Gondwana Cratons.

Location	**Average radioelement concentrations**			**U/Th Ratio**	**Reference**
	Th (ppm)	**U (ppm)**	**K (%)**		
Gneissic Granites, Zimbabwe Craton.	25.3	3.31	3.75	0.13	Present study
Fenitised Granites, Zimbabwe Craton.	62.50	11.16	5.76	0.18	Present study
Porphyritic Granites, Zimbabwe Craton.	62.13	14.40	4.54	0.23	Present study
Pink Granites, Kaapvaal Craton.	15.67	4.84	4.85	0.31	(Moyen et al., 2021)
Sangmelima High-K Granitoids, Congo Craton	16.7	4.8	33,034	0.29	(Shang et al., 2010)
Mirpur Granite, Marwar Craton, India.	54.51	8.06	5.06	0.14	(Scharfenberg et al., 2015)
Balda Granite, Aravalli Craton, India.	23.66	5.84	4.12	0.36	(Scharfenberg et al., 2015)
Armoor Granites, Easter Dharwar Craton, India.	61.16	14.3	4.28	0.23	(Kumar & Ashok, 2024)
Palaeoarchaean Granite, Singhbhum Craton.	10.8	1.4	2.4	0.13	(Ray et al., 2023)
Palaeoarchaean Gneiss, Singhbhum Craton	9.6	1.7	1.8	0.18	(Ray et al., 2023)

Neoarchaean granitoid, Singhbhum Craton	31.1	4.2	3.9	0.14	(Ray et al., 2023)
Porphyritic Granites, Bundelkhand Craton	42.5	8.0	4.3	0.19	(Menon et al., 2003)
Medium-to-coarse grained Granites, Bundelkhand Craton	38.1	8.8	4.6	0.23	(Menon et al., 2003)
Potassic Granite, Bundelkhand Craton	38.5	8.6	4.1	0.23	(Podugu et al., 2017)
Biotite Granite, Bundelkhand Craton	49.5	7.7	3.7	0.16	(Podugu et al., 2017)
TTG Gneiss, Bundelkhand Craton	13.1	3.2	2.3	0.24	(Podugu et al., 2017)
Granites, Doodlakine, Yilgarn Craton, Australia	76.7	10.4	4.0	0.14	(Middleton, 2016)

Moyen et al. (2021) in their study found that the late to post tectonic quartz-monzonite, pink granites intrusive into the Heerenveen Batholith contained enhanced concentrations of thorium, uranium and potassium of 15.67 ppm, 4.84 ppm, and 4.85 %, respectively. The average potassium concentrations of the pink granites in the Heerenveen Batholith, Kaapvaal Craton, South Africa of 4.85 % and the average potassium concentrations of the porphyritic granites and fenitised granites of the AGGTB, Zimbabwe Craton of 4.54 % and 5.76 %, respectively, are comparable. This is expected because both the Kaapvaal Craton and the Zimbabwe Craton are segments of the oldest Precambrian shield of Southern Africa, better known as the Kalahari Craton (3.6-3.0 Ga) (Goodwin, 1996; Tesauro et al., 2026). These late formed cratons and/or granitic intrusives are typically dominated by potassic-rich granite plutonism such as pink monzogranites and syenites (Bucholz & Spencer, 2019; Halla, 2018). The potassic granites of the Kaapvaal Craton, South Africa are believed to be the first granites on Earth which crystallised uraninite, and have been actually proven to be the source of the detrital uraninite for the Dominion Reef and Witwatersrand quartz pebble conglomerate deposits of South Africa (Cuney, 2014; Goodwin, 1996; Plant et al., 1999). The average thorium concentrations of the porphyritic granites (62.13 ppm) and fenitised granites (62.50 ppm) of the AGGTB, Zimbabwe Craton are however markedly higher than the average thorium concentrations of the pink granites in the Heerenveen Batholith, Kaapvaal Craton of 15.67 ppm. With the presence of the aplite granites and pegmatites in the AGGTB, i.e. products of extreme fractionation of felsic magmas which commonly contain enhanced concentrations of the incompatible elements (thorium, potassium and uranium), providing evidences that the Zimbabwe Craton is derived from highly differentiated felsic magmas.

There are several late to post tectonic high potassic granites in many Archaean cratons in the world. Peninsular India, for example is underlain by diverse types of Archaean granitoids including potassic rich granitoids as well. Peninsular India is comprised of five principal cratonic segments, which are: (i) Singhbhum Craton, (ii) Western Dharwar Craton, (iii) Eastern Dharwar Craton, (iv) Bundelkhand Craton and (v) Bastar and Aravalli Craton (Dey & Moyen, 2020). The Singhbhum Craton which is found Eastern India is host to several of these late to post tectonic high potassic granites, and hence comparable to both the Zimbabwe Craton and Kaapvaal Cratons of Southern Africa (Rollinson et al., 2024). A study by Ray et al. (2023) found that the Neoarchaean Granitoids of the Singhbhum Craton contained average concentrations values of thorium, uranium and potassium of 31.1 ppm, 4.2 ppm and 3.9 %, respectively. Whilst the Palaeoarchaean Gneisses of the Singhbhum Craton contained average concentrations of thorium, uranium and potassium of 9.6 ppm, 1.7 ppm, and 1.8 %, respectively. The Palaeoarchaean Granites of the Singhbhum Craton contained average concentrations of thorium, uranium and potassium of 9.6 ppm, 1.7 ppm, and 1.8 %, respectively **(Table 4.7).** Whist there are variations observed in the average concentrations of the radioelements in the different cratons presented in **Table 4.7**, the eU/eTh ratios obtained for all the investigated felsic rocks (gneisses, granites and granites) in these selected cratons were all less than unity, ranging from 0.13 to 0.36. This is consistent with what is expected in Archaean granitoids which are typically characterised by low eU/eTh, which may be attributed to the comparatively low uranium content in their rock units. The average concentrations for thorium in all the selected cratons show a very large range of variation, from 9.6 to 65.5 ppm. However, the concentrations for uranium show a more graded variation, ranging from 1.4 to 14.40 ppm. Hence it can be concluded that most of these Archaean cratons can be considered to be thorium provinces. These results show that the granitic rocks from the AGGTB are comparable, in many respects, to other granitic rocks found in contemporaneous cratons such as the Singhbhum Craton of India, Dharwar Craton of India and the Kaapvaal Craton of South Africa. For example, the average eU/eTh ratios obtained for the potassic-rich granites of the Eastern Dharwar and the Bundelkhand Cratons, India of 0.23 is similar to the eU/eTh ratio obtained for the potassic- rich porphyritic granites in the AGGTB (Kumar & Ashok, 2024; Menon et al., 2003; Podugu et al., 2017). Thus, the most striking and significant feature of all these cratons is the presence of high potassium concentrations. **Table 4.7** shows that the average potassium concentration values for most of the selected former Gondwana Cratons were all above the average concentration value of potassium in the Earth's crust of 2.3% (Rudnick & Gao, 2003). Thus it can be concluded that these Archaean cratons are generally characterised by the numerous occurrences of high potassic granitoids. In addition the uranium concentrations of 3.31 ppm obtained for the gneissic granites in the AGGTB are well below 10 ppm, which is typical of many granitoids. For example, Ray et al. (2023) also found very low uranium concentrations in the Palaeoarchaean Gneiss Granites of the Singhbhum Craton. In conclusion, the data presented in **Table 4.7** demonstrates that the eU/eTh ratios obtained in this study for the felsic rock samples in the AGGTB are typical of the eU/eTh ratios obtained for most Archaean granitoids in former ancient Gondwana cratonic segments from all over the world.

Radiological Hazard Assessment of the felsic rock units in the Archaean Granite-Greenstone Terrane of Bulawayo

Evaluation of Absorbed Dose Rate in Air from Activity Concentrations

The evaluated absorbed dose rates, D (nGy/h) in air at 1 m above the ground surface for a uniform distribution of the naturally occurring radionuclides (^{238}U, ^{232}Th and ^{40}K) in the felsic rock samples from the AGGTB are presented in **Table 4.8.** The absorbed dose rates (D) in air from the older gneissic granitic rock samples in the NGZ, varied from 108.03 to 137.84 nGy/h, with a mean value of 129.92 ± 12.65 nGy/h. This reveals that the mean absorbed dose rate in air for the gneissic granites is almost two times higher than that of the worldwide average absorbed dose rate in air of 59nGy/h (UNSCEAR, 2000). The absorbed dose rates (D) in air from the younger porphyritic granitic rock samples varied from 233.25 to 399.42 nGy/h, with a mean value of 298.86 ± 48.01 nGy/h. This shows that the mean absorbed dose rate in air for the younger porphyritic granites is almost five times higher than that of the worldwide average absorbed dose rate in air of 59nGy/h due to natural terrestrial gamma radiation. The absorbed dose rates (D) in air from the fenitised granitic rock samples, i.e. syenites varied from 183.57 to 429.57 nGy/h, with a mean value of 291.93 ± 85.09 nGy/h. The mean value for the absorbed dose rate in air for the fenitised granites is also considerably higher than the worldwide average value of 59 nGy/h (UNSCEAR, 2000). These results also show that the absorbed dose rates in areas underlain by the fenitised granites and porphyritic granites are comparable.

Table 4. 8: Absorbed dose rate in air at 1 m above the ground for the representative felsic rock samples from the AGGTB.

Felsic Lithotype	**Range of Ambient Dose Equivalent Rate (nGy/h)**	**Average Ambient Dose Equivalent Rate (nGy/h)**
Older Gneissic Granite	108.03 - 137.84	129.92 ± 12.65
Younger Porphyritic Granite	233.25 - 399.42	298.86 ± 48.01
Porphyritic Syenite Quartz	183.57 - 429.57	291.93 ± 85.09
Worldwide average		**59 nGy/h (UNSCEAR, 2000)**

These results show that the absorbed dose rates in the AGGTB for all the three dominant granitic lithotypes are higher than the worldwide average value. However, the areas underlain by the older gneissic granites recorded the lowest values of absorbed dose rates. This is consistent with the fact that these older gneissic granites show signs of hydrothermal alteration as confirmed by the presence of hydrothermal alteration minerals such as sericite and chlorite.

Evaluation of Annual Effective Dose Equivalent (AEDE)

Table 4.9 shows that the AEDE values for the gneissic granitic rock samples in the NGZ, varied from 0.132 to 0.169 mSv/y, with a mean value of 0.159 ± 0.016mSv/y. Whist, the AEDE values for the fenitised granitic rock

samples in the NGZ varied from 0.225 to 0.527 mSv/y, with a mean value of 0.358 ± 0.104 mSv/y. The AEDE values for the porphyritic granitic rock samples in the NGZ varied from 0.286 to 0.490 mSv/y, with a mean value of 0.360 ± 0.059 mSv/y. Hence, the AEDE average values obtained for all the three dominant felsic lithotypes in the AGGTB are all below the worldwide annual effective dose rate from external gamma radiation value of 0.48 mSv/y (UNSCEAR, 2000). These results also show that the AEDE values obtained in the study area vary with lithology, with comparatively lower average AEDE values obtained over the areas underlain by gneissic granites, and comparatively higher values obtained over the areas underlain by both the fenitised and porphyritic granites **(Figure 4.7)**. However, the average AEDE values obtained over the areas underlain by the fenitised and younger porphyritic granites are comparable, i.e. with observed average values of 0.360 mSv/y and 0.358 mSv/y, respectively**.** These findings are in accordance with literature, i.e. the suggestion that both the porphyritic quartz syenites in the SGZ and the younger porphyritic granites in NGZ resulted from the magmatic differentiation and fractionation processes associated with the Matopos Porphyritic Granite Intrusion Event (MPGIE) in the AGGTB, hence these two lithotypes share some remarkable petrological and geochemical properties (Amm, 1965). In conclusion all the AEDE values obtained for the studied felsic rock samples in the AGGTB are significantly below the maximum allowed limit of 1 mSv/y of radiation exposure to the general public (ICRP, 1991). Thus, the ionising radiation caused by gamma radiation exposure from the naturally occurring radionuclides in the AGGTB is unlikely to cause any radiological health risks to the inhabitants.

Table 4.9: Annual effective dose equivalent values for the representative felsic rock samples from the AGGTB.

Felsic Lithotype	**Range of Annual effective dose equivalent (AEDE) (mSv/y)**	**Average Annual effective dose equivalent (AEDE) (mSv/y)**
Older Gneissic Granite	0.132 – 0.169	0.159 ± 0.016
Younger Porphyritic Granite	0.286 – 0.490	0.360 ± 0.059
Porphyritic Syenite Quartz	0.225 – 0.527	0.358 ± 0.104
Worldwide average AEDE for external terrestrial radiation.		**0.48 mSv/y (UNSCEAR, 2000)**

Evaluation of Radium equivalent activity (Ra_{eq})

The radium equivalent activity (Ra_{eq}) which is a measure of the cumulative exposure from the ^{238}U, ^{232}Th and ^{40}K naturally occurring radionuclides in the AGGTB were calculated using equation 3.5, presented in Section 3.3. **Table 4.10** shows that for the gneissic granitic rock samples in the NGZ the radium equivalent activity (Ra_{eq}) varied from 228.05 to 294.45 Bq/kg, with a mean value of 265.32 ± 29.27 Bq/kg. Thus the mean Raeq value for the gneissic granites is less than the world's average of 370 Bq/kg, i.e. satisfies the recommended limit(OECD, 1979).

Table 4.10: Ra_{eq} values for the representative felsic rock samples from the AGGTB.

Felsic Lithotype	Range of radium equivalent activity (Ra_{eq}) (Bq/kg)	Average radium equivalent activity (Ra_{eq}) (Bq/kg)
Older Gneissic Granite	228.05 - 294.45	265.32 ± 29.27
Younger Porphyritic Granite	510.59 - 877.88	648.13 ± 105.76
Porphyritic Syenite Quartz	390.05 - 958.45	639.21 ± 195.77
Recommended maximum Ra_{eq} value		**370 Bq/kg (OECD, 1979)**

For the younger porphyritic granitic rock samples in the NGZ the radium equivalent activity (Ra_{eq}) varied from 510.59 to 877.88 Bq/kg, with a mean value of 648.13±105.76 Bq/kg. Hence the average Ra_{eq} value of 648.13Bq/kg obtained over the areas underlain by the younger porphyritic granites are at least two times higher than the recommended maximum value of 370 Bq/kg (OECD, 1979). For the fenitised granitic rock samples in the SGZ the radium equivalent activity (Ra_{eq}) varied from 390.05 to 958.45 Bq/kg, with a mean value of 639.21±195.77 Bq/kg. This value is approximately twice as much higher than the recommended limit of 370 Bq/kg (OECD, 1979). Thus, the calculated average Ra_{eq} values for the areas underlain by both the porphyritic granites and fenitised granites were higher than the maximum allowed limit of 370 Bq/kg, whilst areas underlain by the gneissic granites in the study area had an average Ra_{eq} value less than the maximum allowed limit of 370 Bq/kg (OECD, 1979).

Evaluation of external hazard index (H_{ext})

The external hazard index (H_{ext}), caused by the gamma-emitting naturally occurring radionuclides in the AGGTB were determined from the obtained activity concentrations for ^{238}U, ^{232}Th and ^{40}K, respectively, using equation 3.6 presented in Section 3.3. **Table 4.11** shows that the He_x values for the areas underlain by the older gneissic granites in the NGZ, varied from 0.61 to 0.80 with a mean value of 0.75 ± 0.08. Thus the average H_{ext} due to the older gneissic granites in the NGZ is below unity, suggesting that these rock units may pose no risk to the radiological health of the local population.

Table 4. 11: H_{ex} values for the representative felsic rock samples from the AGGTB.

Felsic Lithotype	Range of H_{ex} values	Average H_{ex} values

Older Gneissic Granite	0.61- 0.80	0.75 ± 0.08
Younger Porphyritic Granite	1.37 - 2.37	1.75 ± 0.29
Porphyritic Syenite Quartz	1.05 - 2.59	1.73 ± 0.53
Recommended maximum H_{ex} value		**≤ 1 (OECD, 1979)**

Table 4.11 shows that the H_{ex} values for the areas underlain by the fenitised granites in the SGZ varied from 1.05 to 2.59, with a mean value of 1.73 ± 0.53. Thus the average H_{ext} due to the fenitised granites in the SGZ is above unity, suggesting that they may pose a risk to the radiological health of the local population. **Table 4.11** shows that the H_{ex} values for the areas underlain by the younger porphyritic granites in the NGZ varied from 1.37 to 2.37 with a mean value of 1.75 ± 0.29. Thus the mean H_{ext} due to the younger porphyritic granites in the NGZ is above unity, suggesting that they may pose a risk to the radiological health of the local population.

Evaluation of excess lifetime cancer risk (ELCR)

The excess lifetime cancer risk for inhabitants of the AGGTB who are exposed to gamma-emitting naturally occurring radionuclides, were calculated using the computed values of the annual absorbed dose values, as seen in equation 3.7 presented in Section 3.3. The calculated values of ELCR in the areas underlain by the gneissic granites in the NGZ are given in **Table 4.12**. The calculated ELCR values for the gneissic granites in the NGZ varied from 0.46 $x10^{-3}$ to 0.59 $x10^{-3}$, with a mean value of 0.56 ± 0.06 $x10^{-3}$. This value is much higher than the average world ELCR value of 0.29 $x10^{-3}$ (UNSCEAR, 2000). Thus the calculated average ELCR value obtained for the gneissic granites in this study of 0.56 is roughly 1.93 times higher than the world's average for which negligible risk of developing cancer has been stated. This value of 1.93 for the ratio of the calculated average ELCR value in the older gneissic granites in the NGZ to the maximum permissible ELCR value corresponds to an excess percentage risk of 93%. Thus the excess lifetime cancer risk due to the gneissic granites in the NGZ is relatively higher than the world's average.

Table 4.12: The calculated values of ELCR for the representative felsic rock samples from the AGGTB.

Felsic Lithotype	**Range of ELCR values**	**Average ELCR values**
Older Gneissic Granite	$0.46x10^{-3}$ - $0.59x10^{-3}$	0.56 ± 0.06 $x10^{-3}$
Younger Porphyritic Granite	1.00 $x10^{-3}$ - 1.72 $x10^{-3}$	1.26 ± 0.21 $x10^{-3}$
Porphyritic Syenite Quartz	$0.79x10^{-3}$ - $1.85x10^{-3}$	1.26 ± 0.37 $x10^{-3}$

World permissible ELCR value	**$0.29x10^{-3}$ (UNSCEAR, 2000)**

The calculated values of ELCR in the areas underlain by the fenitised granites in the AGGTB are given in **Table 4.12**. The calculated ELCR values for the fenitised granites in the SGZ varied from 0.79 $x10^{-3}$ to 1.85 $x10^{-3}$, with a mean value of 1.26 ± 0.37$x10^{-3}$. This value is much higher than the world permissible ELCR value of 0.29$x10^{-3}$ (UNSCEAR, 2000). Thus the calculated average ELCR value obtained for the fenitised granites in this study of 1.26 is roughly 4.35 times higher than the world's average ELCR value for which negligible risk of developing cancer has been stated. This value of 4.35 for the ratio of the calculated average ELCR value in the fenitised granites to the maximum permissible ELCR value corresponds to an excess percentage risk of 335 %. Thus the excess lifetime cancer risk due to the fenitised granites in the SGZ is significantly higher than the world's average.

The calculated ELCR values for the younger porphyritic granites in the NGZ varied from 1.00$x10^{-3}$ to 1.72$x10^{-3}$, with an average value of 1.26 ± 0.21$x10^{-3}$. This value is more than four times higher than the world permissible ELCR value of 0.29$x10^{-3}$ (UNSCEAR, 2000). Thus the calculated average ELCR value obtained for the younger porphyritic granites in this study of 1.26 ± 0.21$x10^{-3}$ is roughly 4.35 times higher than the world's average for which negligible risk of developing cancer has been stated. This value of 4.35 for the ratio of the calculated average ELCR value in the younger porphyritic granites in the NGZ to the maximum permissible ELCR value corresponds to an excess percentage risk of 335%. Thus the excess lifetime cancer risk due to the younger porphyritic granites in the NGZ is significantly higher than the world's average.

The results from the study show that the calculated ELCR values over the areas underlain by the younger porphyritic granites and the fenitised granites have anomalously high ELCR values, of 1.26 ± 0.21$x10^{-3}$ and 1.26 ± 0.21$x10^{-3}$, respectively. These calculated ELCR values are well outside of the maximum permissible ELCR value of 0.29$x10^{-3}$ M(UNSCEAR, 2000). Thus, the excess percentage risk for developing cancer for both the younger porphyritic granites and the fenitised granites in the AGGTB are the same, both being pegged at about 335%. This can be attributed to the high natural radioactivity content of these two respective lithologic units. This is consistent with the underlying geology for these two regions which are believed to have formed from the same parent magmatic material, hence comparable anomalously high natural radioactivity content, and particularly high activity concentration of ^{40}K content present in both the younger porphyritic granites and the fenitised granites in the AGGTB. As a result the exposure from the gamma-emitting naturally occurring radionuclides in the AGGTB may pose some potential radiological hazard to the inhabitants over the course of their lives. However, the inhabitants of the areas underlain by both the fenitised granites and the younger porphyritic granites have a higher lifetime cancer risk compared to the inhabitants of the areas underlain by the older gneissic granites in the AGGTB. A comparison with the ELCR values obtained from studies carried out in other granitic regions across the world indicates that the ELCR values obtained for the granitic rocks in the AGGTB are actually relatively lower **(Table. 4.13).**

Table 4. 13: Comparison of average ELCR values of felsic rocks from the study with the average ELCR values of similar granitic rock types from other locations in the world.

Location	Average ELCR value ($x10^{-3}$)	Reference
Gneissic granites, Zimbabwe	0.56	Present study
Porphyritic granites, Zimbabwe	1.26	Present study
Fenitised granites, Zimbabwe	1.26	Present study
Egypt	8.57	(El-Arabi, 2007)
Nigeria	1.27	(Akingboye & Ademila, 2019)
Nigeria	1.54	(Ademila, 2020)
South Eastern Desert, Egypt	2.38	(Abdel Gawad et al., 2022)
Eastern Egypt	7.00	(Karim et al., 2021)
Turkey	8.25	(Orgun et al., 2005)
World average value for granites.	4.80	(Qureshi et al., 2016)

Hence, whilst all the ELCR values obtained in this study are higher than the world permissible ELCR value of $0.29x10^{-3}$, they are all below the world average ELCR value for granites of $4.8\ x10^{-3}$ (Qureshi et al., 2016). In addition the ELCR value of $1.26\ x10^{-3}$ obtained for both the fenitised granites and the younger porphyritic granites in the AGGTB of the Zimbabwe Craton are comparable to the ELCR values of $1.27\ x10^{-3}$ and $1.54\ x10^{-3}$ obtained in similar investigations of the granite rocks from the Southwestern Basement Complex of Nigeria, Western African Craton (Ademila, 2020; Akingboye & Ademila, 2019). These observations are consistent with the fact that both the Zimbabwe Craton and the Western African Craton share remarkable physical lithospheric properties, i.e. possess similar temperature and composition profiles as a result of both being underlain by cold depleted lithospheric roots (Finger et al., 2022). In Egypt extensive studies have also been conducted to determine the ELCR values due to granitic rocks in its vast granitic terranes (Abdel Gawad et al., 2022; El-Arabi, 2007; Karim et al., 2021). Most of these studies have revealed that most regions in Egypt are underlain by granitic regions with average ELCR values which are well above the global average values of ELCR for granites. For example results presented in **Table 4.13** demonstrate that very high ELCR values are associated with most granitic rocks from Egypt, particularly in regions underlain by the younger granite plutons of the Precambrian Basement Complex of Eastern Egypt, with anomalously high ELCR values of $7.0\ x\ 10^{-3}$ (Karim et al., 2021).

Conclusion

Twenty four felsic samples from the three main exposed felsic rock units in the AGGTB, namely older gneissic granites, younger porphyritic granites and porphyritic quartz syenites were analysed for their natural radioactivity contents using the gamma-ray (HPGe) technique. The study results have revealed that the activity concentrations of the ^{238}U decay series, ^{232}Th decay series and ^{40}K non series radionuclides in the AGGTB are spatially related to the outcropping felsic rock units (surface geology). Hence, areas that are predominantly underlain by both the younger porphyritic granites and the fenitised granites (i.e. syenites and porphyritic quartz syenites) in the AGGTB have higher activity concentrations of the ^{238}U decay series, ^{232}Th decay series and ^{40}K non series radionuclides compared to areas underlain by the older gneissic granites. This strong correlation of the naturally occurring radionuclides in the ^{238}U decay series, ^{232}Th decay series and ^{40}K non series radionuclides with the underlying geology in the AGGTB is consistent with the behaviour and accumulation of

these naturally occurring radionuclides during granitoid magmatism. Furthermore, these study results have also shown that all the average values of the activity concentrations of the naturally occurring radionuclides in the ^{238}U decay series, ^{232}Th decay series and ^{40}K non series radionuclides in all the felsic rock samples of the AGGTB are higher than the worldwide average activity concentrations of 33 Bq/kg, 45 Bq/kg and 420 Bq/kg for ^{238}U, ^{232}Th and ^{40}K, respectively. The activity concentrations of the ^{40}K non series radionuclides was highest in all the felsic rock samples, which is consistent with the fact that the AGGTB is largely underlain by Late Archaean potassic-rich granitic rocks which is typical of other former Gondwana cratonic regions elsewhere in the world. Evidence of involvement of metasomatic activity of the radioelements or fractionation is observed particularly, for the older gneissic granites in the AGGTB as demonstrated by the invariably lower eU/Th values. The radiological hazard parameters findings suggest that the activity concentrations of the ^{238}U decay series, ^{232}Th decay series and ^{40}K non series radionuclides may pose radiological health risks to the inhabitants of the AGGTB, particularly in areas underlain by both the younger porphyritic granites and the fenitised granites (i.e. syenites and porphyritic quartz syenites) in the AGGTB.

Declarations

Author Contributions: Conceptualization: R.T.M and M.M.; Methodology: R.T.M. and M.M.; Supervision: M.M.; Investigation: R.TM; Data curation: R.T.M.; I.M.; Formal analysis: R.T.M., I.M.; Validation: I.M.; Writing original draft preparation: R.T.M.; Writing review and editing: R.T.M., M.M. and I.M. All authors have read and agreed to the published version of the manuscript.

Conflict of Interest: The authors declare no conflicts of interests.

Consent for publication: All the authors consented and approve the publication of the manuscript.

Funding: The authors would like to acknowledge the financial support from the National University of Science and Technology (NUST), provided in the form of a NUST Research Board Grant. Appreciation also goes to the North West University (NWU) for providing Robin Tinavo Mashingaidze with a NWU Doctoral Bursary Award. Finally, we acknowledge the Radiation Protection Authority of Zimbabwe (RPAZ) for the provision of the HPGe Gamma-Ray Spectrometry services.

Institutional Review Board Statement: The research was approved by the North West University (NWU), South Africa, Faculty of Natural and Agricultural Sciences Ethics Committee (FNASREC) under ethics number NWU-01241-22-A9: dated: 26 September 2025 and as a low risk.

Data Availability Statement: Data are shared in this research article. Further, enquiries can be directed to the corresponding author.

Acknowledgments: The authors also express their gratitude to the Radiation Protection Authority of Zimbabwe (RPAZ) for granting access to and use of their laboratory facilities.

References

Abdel Gawad, A. E., Ali, K. G., Wahed, A. A. A., Alsafi, K., Khafaji, M., Albahiti, S., Khalil, M., Masoud, M. S., & Hanfi, M. Y. (2022). Excess Lifetime Cancer Risk Associated with Granite Bearing Radioactive Minerals and Valuable Metals, Monqul Area, North

Eastern Desert, Egypt. *Materials*(15). https://doi.org/10.3390/ma15124307

Ademila, O. (2020). Evaluation of rock radiation hazards for construction applications in parts of southwest Nigeria. *Journal of Scientific Research*, *64*(2). https://doi.org/10.37398/JSR.2020.640205

Aghdam, M. M., Crowley, Q., Rocha, C., Dentoni, V., DaPelo, S., Long, S., & Savatier, M. (2021). A Study of Natural Radioactivity Levels and Radon/Thoron Release Potential of Bedrock and Soil in Southeastern Ireland. *International Journal of Environmental Research and Public Health*, *18*. https://doi.org/10.3390/ijerph18052709

Akingboye, A. S., & Ademila, O. (2019). In situ natural radioactivity and radiological hazard assessments of granite gneiss outcrops in parts of the Southwestern Basement Complex of Nigeria. *Journal of Natural Hazards and Environment*, *5*(2), 214-223.

Alharbi, S. (2016). *Measurement and Monitoring of Naturally Occurring Radioactive Materials for Regulation* Queensland University of Technology.

Amm, F. L. (1965). *The Geology of the Country around Bulawayo: Southern Rhodesia Geological Survey Bulletin No.35*. Government Printers.

Bajoga, A. D. (2016). *Evaluation of Natural and Anthropogenic Radioactivity in Environmental samples from Kuwait Using High-resolution Gamma-ray Spectrometry* University of Surrey]. Guildford, United Kingdom.

Barretto, P. M. C., & Tassinari, C. C. G. (1992). Uranium in granitoids: Recognition criteria of uranium provinces in Brazil New developments in uranium exploration, resources, production and demand: IAEA-TECDOC-650 Vienna.

Baz, S. S., Al-Ghamdi, A. H., Fakeha, A. A., & Alamoudi, Z. M. (2015). Natural radioactivity measurement and evaluation of radiological hazards in some environmental materials from Aswan area, Upper Egypt. *Journal of American Science*, *11*.

Bezuidenhout, J. (2019). The relationship among naturally occurring radionuclides, geology, and geography: Tsodilo Hills, Botswana. *Journal of Radiation Research and Applied Sciences, VOL. 12, NO. 1*, 93–100.

Bucholz, C. E., & Spencer, C. J. (2019). Strongly Peraluminous Granites across the Archean–Proterozoic Transition. *Journal of Petrology*, *60*, 1299–1348. https://doi.org/10.1093/petrology/egz033

Canberra. (2006). *Genie™ 2000 Spectroscopy Software: Operations*.

Carlson, R., Garçon, M., O'neil, J., Reimink, J., & Rizo, H. (2019). The nature of Earth's first crust. *Chemical Geology, Elsevier*, *530*. https://doi.org/10.1016/j.chemgeo.2019.119321

Chen, C. J., & Lin, Y. M. (1996). Assessment of building materials for compliance with regulations of ROC. *Environment International*(22), 221-226. https://doi.org/10.1016/S0160-4120(96)00111-0

Christodoulides, G., Tzortzis, M., & Tsertos, H. (2003). Gamma-ray measurements of naturally occurring radioactive samples from Cyprus characteristic geological rocks. *Radiation Measurements*(37), 221-229.

Cinelli, G., De Cort, M., & Tollefsen, T. (Eds.). (2019). *European Atlas of Natural Radiation,* (1st ed.). Publications Office of the European Union. https://doi.org/10.2760/46388.

Cumberland, S. A., Douglas, G., Grice, K., & Moreau, J. W. (2016). Uranium mobility in organic matter-rich sediments: A review of geological and geochemical processes. *Earth-Science Reviews*, *159*, 160-185. https://doi.org/10.1016/j.earscirev.2016.05.010

Cuney, M. (2014). Felsic magmatism and uranium deposits. *Bulletin de la Societe Geologique de France*, *185*.

Dey, S., & Moyen, J. F. (2020). Archean Granitoids of India: Windows into early Earth tectonics. *Geological Society, London, Special Publications,*. https://doi.org/doi.org/10.1144/SP489-2020-155

Dina, N. T., Das, S. C., Kabir, M. Z., Rasul, M. G., Deeba, F., Rajib, M., Islam, S. M., Hayder, M. A., & Ali, A., M. (2022). Natural radioactivity and its radiological implications from soils and rocks in Jaintiapur area, Northeast Bangladesh. *Journal of Radioanalytical and Nuclear Chemistry 331:*, 4457–4468.

Dumisa, S. S., Bybee, G. M., Nex, P. A. M., & Jogee, B. A. (2024). The petrogenesis of orbicular granites in the Diana's Pool area, Zimbabwe. *Geological Society of South Africa*, *127*, 1-16. https://doi.org/10.25131/sajg.127.0021

Eikenberg, J. (2002). *Radium isotope systematics in nature: applications in geochronology and hydrogeochemistry* Swiss Federal Institute of Technology (ETH) Zürich]. Villigen.

El-Arabi, A. M. (2007). 226Ra, 232Th and 40K concentrations in igneous rocks from the eastern desert, Egypt and its radiological implications. *Radiation Measurements*, *42*, 94-100.

Finger, N. P., Kaban, M. K., Tesauro, M., Mooney, W. D., & Thomas, M. (2022). A Thermo-Compositional Model of the African Cratonic Lithosphere. *Geochemistry, Geophysics, Geosystems*, *23*.

Garson, M. S. (1995). *The Geology of the Bulawayo Greenstone Belt and the surrounding granitic terrain*.

Goodwin, A. M. (1996). *Principles of Precambrian Geology* (Second ed.). Academic Press.

GSZ. (2024). *Summer Symposium: Field Guide Hillside Syenite Diana's Pool Orbicular Granite*.

Halla, J. (2018). Highlights on Geochemical Changes in Archaean Granitoids and Their Implications for Early Earth Geodynamics. *Geosciences*, *8*(353). https://doi.org/10.3390/geosciences8090353

Hofmann, A., Bolhar, R., Kuznetsov, A. B., Jodder, J., Butler, M., & Nguyen, A. (2023). A craton-wide geochemical study of Neoarchaean carbonate rocks of Zimbabwe. *Chemical Geology, Elsevier*, *634*(121587).

IAEA. (1989). *Uranium deposits in magmatic and metamorphic rocks*

IAEA. (2003). *Guidelines for radioelement mapping using gamma ray spectrometry data* (IAEA-TECDOC-1363, Issue.

IAEA. (2004). *Radiation, people and the environment*. International Atomic Energy Agency.

ICRP. (1991). *ICRP Publication 60. 1990 Recommendations of the International Commission on Radiological Protection*. P. Press.

Isinkaye, M. O., & Emelue, H. U. (2015). Natural radioactivity measurements and evaluation of radiological in sediment of Oguta Lake, South East Nigeria. *Journal of Radiation Research and Applied Sciences*, 459-469.

Jelsma, H. A., & Dirks, P. H. G. M. (2000). Tectonic evolution of a greenstone sequence in northern Zimbabwe: sequential early stacking and pluton diapirism. *Tectonics*, *19*(No. 1).

Karim, M. A., Gafaar, I., ElHalim, E. A., M., H., & ElDine, N. W. (2021). Natural radioactivity and radiological implications of granite rocks, ElSela area, Southeastern Desert, Egypt. *Journal of Radioanalytical and Nuclear Chemistry*. https://doi.org/10.1007/s10967-021-07992-6

Kerur, B. R., Rajeshwari, T., Nagabushna, N. M., Kumar, A., Narayani, S., & Rekha, A. K. (2010). Radioactivity measurement in the granites of North Karnataka, India and its radiological implications. *Indian Journal of Physics 84*, 1467-1480.

Khan, A. J., Syed, U. F., Roselan, A. L., & Costello, C. A. (2023). Uranium Series Disequilibrium and Precision Measurement of Radionuclides Activity in Sediment Sample Using Low Background Gamma Spectrometry. *Journal of Geoscience and Environment Protection*, *11*, 119-140. https://doi.org/10.4236/gep.2023.1110010

Kumar, A. A., & Ashok, C. (2024). Geochemistry and mineral chemistry of the armoor granitoids, eastern dharwar craton: implications for the redox conditions and tectono-magmatic environment. *Acta Geochimica*, *43*, 110-133.

Laubenstein, M., & Lawson, I. (2020). Low Background Radiation Detection Techniques and Mitigation of Radioactive Backgrounds. *Frontiers in Phys. 8:577734.*

Manikyamba, C., Upadhyay, D., & Mohan, M. R. (2024). Archean crustal evolution and craton formation in peninsular India: new insights from the Singhbhum, Dharwar and Bastar Cratons. *Proceedings of the Indian National Science Academy*, *90*, 167-195. https://doi.org/10.1007/s43538-024-00254-5

Mareschal, J. a. J., C. (2014). *Constraints on Crustal Heat Production from Heat Flow Data* (Vol. 4). Elsevier.

Mason, B., & Moore, C. B. (1982). *Principles of Geochemistry*. John Wiley and Sons Ltd.

Menon, R., Kumar, P. S., Reddy, G. K., & Srinivasan, R. (2003). Radiogenic heat production of late Archaean Bundelkhand granite and some Proterozoic gneisses and granitoids of central India. *Current Science*, *85*, 634–638.

Middleton, M. F. (2016). Radiogenic Heat Generation in Western Australia — Implications for Geothermal Energy. In B. I. Ismail (Ed.), *Advances in Geothermal Energy*. Intech. https://doi.org/dx.doi.org/10.5772/61963

Moyen, J. F., Zeh, A., Cuney, M., Dziggel, A., & Carrouée, S. (2021). The multiple ways of recycling Archaean crust: A case study from the ca. 3.1 Ga granitoids from the Barberton Greenstone Belt, South Africa. *Precambrian Research*. https://doi.org/10.1016/j.precamres.2020.105998

Nishimori, R. K., Ragland, P. C., Rogers, J. J. W., & Greenberg, J. K. (1977). *A Report to the Energy Research and Development Administration on Uranium Deposits in Granitic rocks*.

OECD. (1979). *Report by a Group of Experts of the OECD Nuclear Energy Agency*.

Omonya, W. L. (2021). *Human exposure and associated risks due to natural radioactivity and heavy metals in ortum, West Pokot County, Kenya* KENYATTA UNIVERSITY].

Orgun, Y., Altınsoy, N., Gultekin, A. H., Karahan, G., & Celebi, N. (2005). Natural radioactivity levels in granitic plutons and groundwaters in Southeast part of Eskisehir, Turkey. *Applied Radiation and Isotopes* (63), 267–275.

Plant, J. A., Simpson, P. R., Smith, B., & Windley, B. F. (1999). Uranium Ore Deposits - Products of the Radioactive Earth. In P. C. Burns & R. J. Finch (Eds.), *Uranium: Mineralogy, Geochemistry, and the Enviroment* De Gruyter. https://doi.org/10.1515/9781501509193

Podugu, N., Ray, L., Singh, S. P., & Roy, S. (2017). Heat flow, heat production, and crustal temperatures in the Archaean Bundelkhand craton, north-central India: Implications for thermal regime beneath the Indian shield. *Journal of Geophysical Research: Solid Earth*, *122*, 5766–5788. https://doi.org/10.1002/2017JB014041

Qureshi, A. A., Siddiqui, R. U. H., Manzoor, S., Rana, A. N., & Waheed, A. (2016). Radiological implications of Nagarparkar granite, Pakistan, as a building material. *Radioprotection*, *51*, 255-263.

Rajesh, H. M., Mukhopadhyay, J., Beukes, N. J., Gutzmer, J., Belyanin, G. A., & Armstrong, R. A. (2009). Evidence for an early Archaean granite from Bastar craton, India. *Journal of the Geological Society*, *166*, 193-196. https://doi.org/10.1144/0016-76492008-089

Ray, L., Dey, S., & Chopra, N. (2023). Radioelement abundances and heat production in the Paleoarchaean and early Neoarchaean granitoids of the Singhbhum Craton, eastern India: Thermal and geodynamic implications. *The Royal Astronomical Society*.

Rikhvanov, L. P. (2019). Using Radioactive Elements and the Th/U Ratio in Study of the Geochemical Typification of Granitoids and Their Intrusive Character. *Russian Geology and Geophysics*, *60*, 1018-1025. https://doi.org/10.15372/RGG2019067

Rollinson, H., Chagondah, G., & Hofmann, A. (2024). The late Archaean granite paradox: A case study from the Zimbabwe Craton. *Precambrian Research 410*. https://doi.org/10.1016/j.precamres.2024.107491

Rudnick, R. L., & Gao, S. (2003). *Composition of the continental crust. Treatise on Geochemistry*. Elservier-Pergamon.

Salupeto-Dembo, J., SzabóKrausz, Z., Völgyesi, P., Kis, Z., Szab, C. . (2020). External radiation exposure of the Angolan population living in adobe houses. *Journal of Radioanalytical and Nuclear Chemistry*(323), 353–364. https://doi.org/10.1007/s10967-019-06920-z

Scharfenberg, L., De Wall, H., Schobel, S., Minor, A., Maurer, M., Pandit, M. K., & Sharma, K. K. (2015). In situ gamma radiation measurements in the Neoproterozoic rocks of Sirohi region, NW India. *Journal of Earth System Science*, *124*, 1223–1234.

Shang, C. K., Liégeois, J. P., Satir, M., Frisch, W., & Nsifa, E. N. (2010). Late Archaean high-K granite geochronology of the northern metacratonic margin of the Archaean Congo craton, Southern Cameroon: Evidence for Pb-loss due to

non-metamorphic causes. *Gondwana Research*. https://doi.org/10.1016/j.gr.2010.02.008

Sharma, A. K., Sahoo, S. K. and Gupta, K. (2025). Assessment of outdoor gamma radiation levels and exposure assessment in Alwar district of Rajasthan, India. *Radiation Protection and Environment*, *48*, 46-53.

Sohrabi, M. (2013). World high background natural radiation areas: Need to protect public. *Radiation Measurements*, 166-171.

Sreedharan, H., & Geetha, A. C. (2016). Review on studies in high background radiation areas (HBRAs) of various parts of the world. *International Journal of Advanced Research in Biological Sciences, Vol 3, Issue 8* 163-169.

Taylor, P. N., Jones, N. W., & Moorbath, S. (1984). Isotopic Assessment of Relative Contributions from Crust and Mantle Sources to theMagma Genesis of Precambrian Granitoid Rocks. *Philosophical Transactions of the Royal Society of London. Series A, Mathematicaland Physical Sciences,*, *310*.

Tesauro, M., Kaban, M. K., & Youssof, M. (2026). Thermal and compositional state of the South African Cratonic Region from seismic and gravity models. *Global and Planetary Change 259*. https://doi.org/10.1016/j.gloplacha.2026.105360

Turner, P. (1991). *B93:Bulawayo*. Harare, Zimbabwe Government Printers.

Tye, A. M., Milodowski, A. E., & Smedley, P. L. (2017). *Distribution of Natural Radioactivity in the Environment. British Geological Survey Open Report, OR/17/01*. N. E. R. C. (NERC).

UNSCEAR. (2000). *Sources and effects of ionzing radiation*.

UNSCEAR. (2018). *Sources, Effects and Risks of Ionizing Radiation. United Nations Scientific Committee on the Effects of Atomic Radiation* (UNSCEAR 2017: Report to the General Assembly, with Scientific Annexes B, Issue.

Wilson, J. F., Nesbitt, R. W., & Fanning, C. M. (1995). Zircon geochronology of Archaean felsic sequences in the Zimbabwe craton: a revision of greenstone stratigraphy and a model for crustal growth. In M. E. Coward & A. C. Ries (Eds.), *Early Precambrian Processes* (Vol. No. 95, pp. 109-126). Geological Society Special Publication.

Xhixha, M. (2013). *New gamma-ray spectrometry methods for estimating K, U, Th concentrations in rocks of the Sardinia Batholith*.

Zubair, M., & Shafiqullah. (2020). Measurement of natural radioactivity in several sandy-loamy soil samples from Sijua, Dhanbad, India. *Heliyon 6 e0340*.